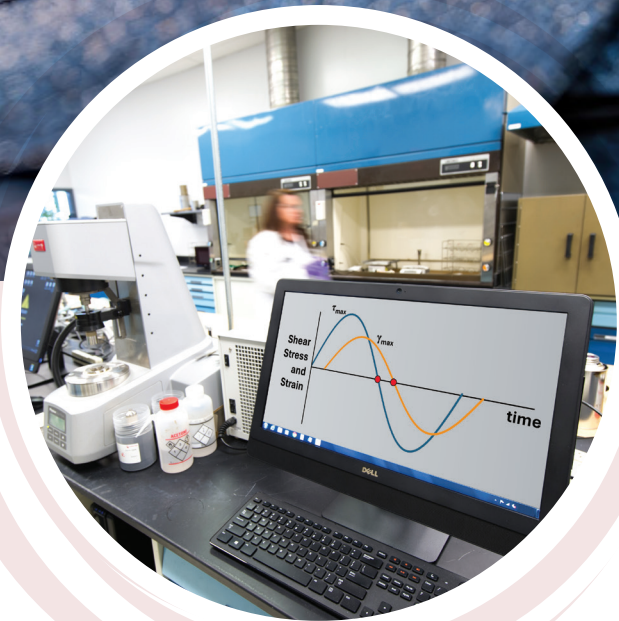


UNDERSTANDING AND IMPROVING THE DURABILITY OF ASPHALT SHINGLES



aif
Asphalt Institute
Foundation®

Final Report

2024-05-10 version

AIF Research Project 22-03

**Understanding and Improving the
Durability of Asphalt Shingles**

**Phase 1 – Investigation of the Rheological Properties of
Binders Recovered from Asphalt Shingles and their
Relation to Performance**

Geoffrey M. Rowe, Abatech, Inc.
Wesley G. Cooper, Asphalt Institute
R. Michael Anderson, Asphalt Institute

for
Asphalt Institute Foundation
and
State Farm Mutual Automobile Insurance Company

December 2023

Foreword

The objective of this research project was to advance the science around the durability of asphalt shingles, specifically by achieving a better understanding of the properties of the coating asphalt used in residential roofing and how those properties affect performance of the shingle in service.

Phase 1 – the subject of the report – was designed to evaluate the effects of aging of the roofing asphalt binder and the change in physical properties as a result which may lead to brittleness, cracking, and loss of granule adhesion. These characteristics are associated with hail damage which is a major performance concern for consumers and insurers.

The research was sponsored by the Asphalt Institute Foundation, through a grant from State Farm Mutual Automobile Insurance Company.

The Asphalt Institute Foundation is a public charity, not-for-profit organization that meets the requirements of Internal Revenue Code Section 501(c)(3). The Foundation conducts strategic research and educational activities that are designed to advance and improve both the liquid asphalt industry and the welfare of the general public.



Executive Summary

The objective of this research project was to advance the science around the durability of asphalt shingles, specifically the properties of the coating asphalt used in residential roofing. Although multiple phases were envisioned at the start of the research, Phase 1 – the subject of the report – was designed to evaluate the effects of aging of the roofing asphalt binder and the change in physical properties as a result which may lead to brittleness, cracking, and loss of granule adhesion. These are associated with hail damage which is a major performance concern for consumers and insurers. Phase 1 was intended to focus on identifying one or more parameters, preferably determined using standard asphalt materials testing equipment, which are hypothesized to relate to the durability of asphalt shingles.

The findings from Phase 1 of this research project indicate that rheology and failure tests can be used to characterize the effects of aging and the change in physical properties of roofing asphalt binders that may be related to shingle performance and durability – specifically damage (cracking) and loss of granule adhesion resulting from the impacts of hail. The three parameters best correlated with performance in each category appear to be:

- the phase angle (δ) at a constant modulus (10 MPa);
- the temperature which, when evaluated at 10 rads, corresponds to a δ of 27°; and
- the Fatigue/Fracture Performance Ratio (FFPR) and yield energy determined from the modified Binder Yield Energy Test (BYET) procedure (now renamed as MOSS – **MO**notonic **S**hear **S**trength test).

The test procedures can be conducted using the Dynamic Shear Rheometer (DSR) with conventional 8-mm parallel plate geometry.

Although Phase 1 was successful, its limited scope means that additional work is needed to fully validate the findings and to ultimately assist suppliers and purchasers of asphalt shingles in understanding what parameters they need to consider to provide enhanced durability and a longer life cycle for asphalt shingles.

Recommendations to consider as an extension to Phase 1 of the research are:

- Extend the findings using additional roofing materials from one or more aging farms and other related studies to evaluate the correlations that exist between rheological properties and performance.
- Continue to improve and re-evaluate promising test procedures such as the MOSS test.
- Evaluate the need to adapt criteria to changing environmental conditions.

Investigation of the Rheological Properties of Binders Recovered from Asphalt Shingles and their Relation to Performance

- Contents -

- Introduction..... 4
 - Components of an Asphalt Shingle and Relationship to Performance..... 4
 - Research Objective..... 5
- Experimental Plan and Materials 6
- Test Methods..... 10
 - Rheology 10
 - Dynamic Shear Rheometer 10
 - Bending Beam Rheometer 11
 - Combination of Data using RHEA 14
- Ultimate Tests 15
 - Asphalt Binder Cracking Device (ABCD) 15
 - Simplified Double-Edge-Notched Tension (SDENT) Test 17
 - Binder Yield Energy Test (BYET) 18
 - Poker Chip Test 20
- Rheological Analysis 22
- Parametric Analysis 26
 - Rheological Parameters 26
- Ultimate Properties..... 30
 - Asphalt Binder Cracking Device (ABCD) 30
 - Simplified Double-Edge-Notched Tension (SDENT) Test 31
 - Modified Binder Yield Energy Test (modified BYET) 35
 - Poker Chip Test 38
- Discussion 43
 - ABCD 43
 - Modified BYET and Rheological Properties..... 44
 - FFPR and Approach Considered in SDENT and MBYET 45

Performance Review	49
Summary	51
Rheology	51
Ultimate tests	51
Recommendations for Additional Study	53
Extension to Additional Roofing Materials	53
Test Method Improvements	53
Climatic Assessment.....	53
Acknowledgments.....	54
Disclaimer	54
References.....	55
Appendix A.....	57
Draft Procedure for Determining the Fatigue/Fracture Performance Ratio (FFPR) using a Dynamic Shear Rheometer (DSR).....	57

Introduction

Achieving a sustainable future for the asphalt roofing industry depends in part on engaging in the principles of sustainable materials management (SMM) which offers a “...systemic approach to using and reusing materials more productively over their entire life cycles” (EPA, 2023). With performance warranties extending twenty or more years for steep-slope roofing applications (shingles), long-term performance must be a consideration as part of the SMM practices. The long-term performance of asphalt shingles – particularly with respect to durability – needs to be better understood and quantified so that asphalt shingles will have enhanced durability, resulting in an extension of their useful service life and a delay in the onset of end-of-life management activities such as reuse and recycling.

A Call for Proposals from the Asphalt Institute Foundation (AIF) in 2021 sought ideas on improving the sustainability of roofing asphalt materials considering all phases of the material life cycle. In the *Use* phase, a key goal was identifying the characteristics and properties needed to design and manufacture more durable asphalt roofing materials. The call for proposals further asked: how can the performance and life cycle of asphalt shingles be improved to sustainably compete with alternative products in the market?

As the AIF Call for Proposals was being developed in 2021, State Farm Mutual Automobile Insurance Company simultaneously expressed interest in partnering with the asphalt industry to understand how to improve the quality of asphalt shingles – noting that the standard industry measures using product weight and warranty periods are not direct measures of quality. If an asphalt shingle can be made more resistant to distresses, the time to replacement can be extended, resulting in ultimate cost savings to homeowners and less material requiring end-of-life-management practices (reuse, recycle, landfill).

Components of an Asphalt Shingle and Relationship to Performance

Asphalt shingles consist of the following components (ARMA, 2023):

- Fiberglass mat;
- Coating asphalt;
- Mineral fillers;
- Granules; and
- Back surfacing.

The fiberglass mat provides the backbone of the shingle, needed for handling and durability. The coating asphalt serves to provide waterproofing characteristics and holds the granules in place. The granules, in turn, protect the asphalt from degradation that would occur from prolonged exposure to UV light. The mineral fillers help increase the asphalt’s resistance to fire, and can improve weathering, flexibility and durability. The back surfacing allows shingles to be more easily manufactured and stored (ARMA, 2023).

The durability of an asphalt shingle is most related to the coating asphalt since it comprises a substantial portion of the shingle and is significantly affected by oxidation and UV exposure, unlike the other components – the granules and mineral fillers – which exist to assist the coating asphalt. As such, it is expected that the properties of the coating asphalt will be important to the performance of the shingle.

Research Objective

A key objective of this research is to advance the science around the durability of asphalt shingles, specifically the properties of the coating asphalt used in residential roofing. The goal is to achieve public sector understanding of the science behind asphalt shingle aging that that would not only benefit the roofing industry, but would also provide:

- A scientific basis from which to advocate for use of better materials, formulations, and designs.
- A forum to collaborate with industry for better test standards.
- New insight into the development of effective accelerated aging tests and methods.
- Opportunity for the insurance industry to underwrite to more accurate quality and performance expectations.
- Opportunity for the insurance industry to provide consumers with a better measure of quality and durability than present manufacturer warranty, weight, and cost marketing.
- Opportunity to extend the window of good performance against hail, wind, and the effects of natural aging and weathering.

This research is expected to require multiple phases to reach a successful conclusion. Phase 1 of the research, the subject of this report, was designed to evaluate the aging of the asphalt binder and the change in physical properties as a result of aging which may lead to brittleness, cracking, and loss of adhesion to granules. Phase 1 was intended to focus on identifying one or more parameters, preferably determined using standard asphalt materials testing equipment, that are hypothesized to relate to the durability of asphalt shingles.

Experimental Plan and Materials

To accomplish the Phase 1 research objectives, the research team chose to take advantage of the field aging site and samples available at State Farm’s facility in Bloomington, Illinois called The Research and Innovation Laboratory (TRAIL). The research team initially visited TRAIL in May 2022 to review the field aging sites (aging farm) and discuss a possible sampling and testing program. The overall layout of the aging farm at TRAIL is shown in Figure 1. Figure 2 and Figure 3 show various views of the test racks at the farm. Each roof location was positioned so that shingles would have both a northern and southern exposure.

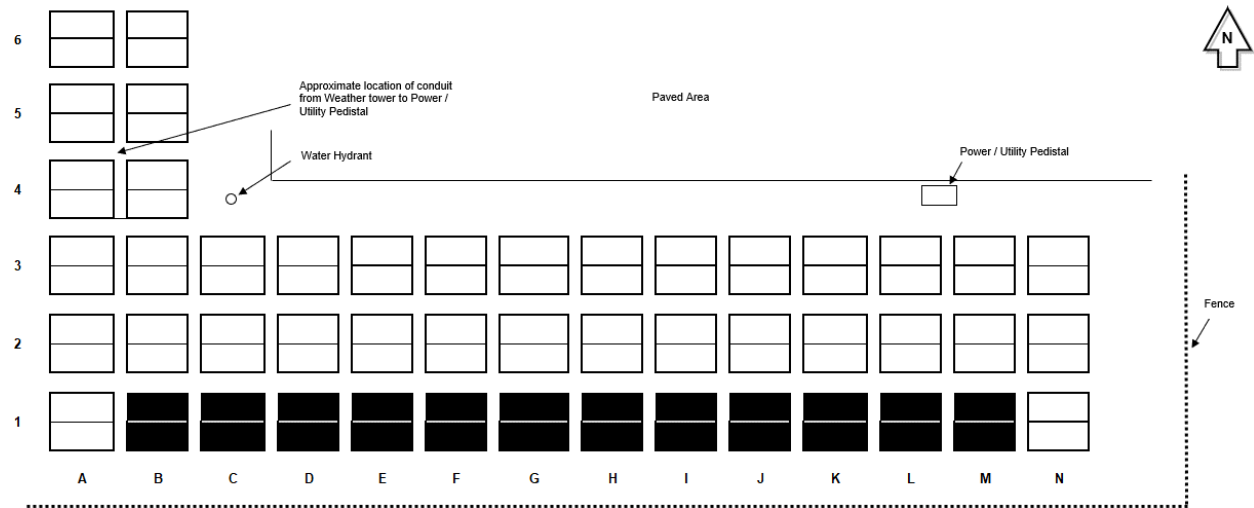


Figure 1: Schematic of Bloomington, IL Aging Farm at State Farm TRAIL



Figure 2: Bloomington, IL Aging Farm at State Farm TRAIL



Figure 3: Asphalt Shingles In-Service at Bloomington, IL Aging Farm (State Farm TRAIL)

Asphalt shingles were harvested in October 2022 from the northern and southern-facing sides of the test racks (roofs) at the Bloomington, IL aging farm at TRAIL, as indicated by the black shaded racks (B to M) in Figure 1 and Table 1. All samples were originally installed in October and November 2002. In addition to the aged samples, State Farm provided original, unaged samples that had been stored in boxes in a temperature-controlled laboratory.

After approximately 5.5 years in service, in May 2008, State Farm removed panels from the asphalt shingle test racks and subjected them to impact testing following the Underwriters Laboratory (UL) Test Standard 2218, *Standard for Impact Resistance of Prepared Roof Covering Materials*. The results are shown in Table 1.

Table 1: UL 2218 Impact Resistance After 5.5 Years of Exposure at TRAIL Aging Farm

Test results (Impact Classification)			UL 2218 (Specific Test Data by Exposure)									
			Northern exposure					Southern exposure				
			North	South	Impact Locations	Total Impact Pts.	Locations w/Noted Damage		Impact Locations	Total Impact Pts.	Locations w/Noted Damage	
No.	%	No.					%					
B3	11/08/02	04/29/08	3	2	12	24	3	25%	15	30	5	33%
C3	11/06/02	04/29/08	0	0	4	8	2	50%	4	8	2	50%
D3	11/12/02	05/28/08	0	0	8	16	5	63%	4	8	3	75%
E3	11/13/02	05/28/08	1	0	14	28	1	7%	15	30	8	53%
F3	11/04/02	05/28/08	2	2	12	24	4	33%	12	24	4	33%
G3	10/31/02	05/28/08	1	2	13	26	3	23%	8	16	1	13%
H3	11/01/02	05/28/08	2	2	13	26	8	62%	12	24	7	58%
I3	10/28/02	05/28/08	0	0	4	8	2	50%	8	16	5	63%
J3	10/22/02	05/28/08	0	0	4	8	4	100%	5	10	4	80%
K3	10/22/02	05/28/08	0	0	4	8	4	100%	4	8	4	100%
L3	10/17/02	05/28/08	0	0	5	10	4	80%	4	8	4	100%
M3	10/21/02	05/28/08	0	0	4	8	4	100%	4	8	4	100%
Totals:					97	194	44	45%	95	190	51	54%

In addition to the UL2218 testing, State Farm conducted additional ASTM standard physical property testing – including ASTM standards D3462, D4977, D4932, D4932, and D5683 – to fully understand the performance of the shingles in service. Those results are not reported as part of this study.

Four test racks representing two polymer modified materials and two oxidized materials were selected for evaluation. These were chosen based on the range of performance from the five-year evaluation provided by State Farm. Northern and southern exposures were chosen from two of the test racks (G1 and M1). For the other two test racks (B1 and J1), just the southern exposure was chosen for evaluation. The test plan to evaluate two test racks with northern and southern exposure and two test racks with only the southern exposure provided the research team with the opportunity to evaluate six samples with varying composition and aging performance. The corresponding unaged test rack samples were also selected for extraction/recovery. In this case, however, there were only four materials since the shingle orientation (Northern/Southern exposure) is not a variable. With the unaged and aged samples there were a total of ten distinct samples evaluated representing different materials, aging and exposure. Multiple sample IDs were provided for the unaged samples but in reality, they were expected to have identical properties. Table 2 shows the information on the samples selected for evaluation in the research project. Information on manufacturer and product name were not included.

Table 2: Samples Selected for Evaluation

Sample ID	Test Rack ID	Age (Years) ^a	Orientation	Sampling Location	Shingle Type	Asphalt Type
AGED						
6	B1	19.9	South	Right	Laminated	Modified
33	G1	19.9	North	Right	Laminated	Modified
36			South	Right		
53	J1	20.0	South	Left	Laminated	Oxidized
68	M1	20.0	North	Left	Three-Tab	Oxidized
71			South	Left		
UNAGED						
1 and 4	B1	0 ^b	n/a	n/a	Laminated	Modified
24 and 25	G1	0 ^b	n/a	n/a	Laminated	Modified
40 and 41	J1	0 ^b	n/a	n/a	Laminated	Oxidized
53, 54, and 56	M1	0 ^b	n/a	n/a	Three-Tab	Oxidized

^a Environmental aging in service.

^b Samples in boxes in TRAIL storage area.

Sufficient sample sizes were chosen (about 750-1040 grams) so that the recovery procedure would yield approximately 150-260 grams of recovered asphalt binder, assuming approximately 20-25% asphalt binder in each shingle.

In a typical extraction/recovery procedure conducted on asphalt paving mixtures and cores, approximately 100 grams of asphalt binder are recovered (assuming 2000 grams of asphalt paving mix with approximately 5% asphalt binder content). To keep the solvent-binder ratio approximately the same as in recovering asphalt paving mixtures, the research team elected to perform two recovery procedures for each sample, resulting in a total of 20 recovery procedures conducted ((6 aged samples + 4 unaged samples) x 2). The soak time in the solvent was limited to one hour. A preliminary trial run performed on a sample of retail

shingles (from Lowes) indicated that this seemed to be sufficient time to remove the asphalt binder while minimizing the risk of inducing excessive solvent hardening in the recovered asphalt binder.

Recovered asphalt binder from each recovery procedure was kept separate, resulting in two replicates of approximately 75-130 grams for each of the ten samples. The research team preferred this approach to allow for variability to be considered as a function of recovery and test procedure, if desired.

The sample reference system followed in the tables and graphics of the results has been simplified to test rack ID and orientation/exposure (N = north, S = south and B = box sample), with a sample ID included in parentheses. Thus, M1-B (54) identifies material associated with a sample taken from shingles used on test rack number M1. The “B” indicates that the sample was not environmentally aged but was an unaged sample taken from the boxes in storage in the TRAIL. The “54” provides a sample ID number. It should be noted that two sets of sample numbers exist, one for rack samples and the second for the box samples, resulting in a duplicate sample ID number in one case.

Test Methods

Rheology

Rheological testing made use of two test pieces of equipment: the dynamic shear rheometer (DSR) and the bending beam rheometer (BBR) used in characterizing paving grade asphalt binders. Analysis was conducted using the RHEA software. The methods and analysis are described in detail in this section.

Dynamic Shear Rheometer

Dynamic shear rheometer (DSR) testing, shown in Figure 4, was conducted using 4-mm, 8-mm and 25-mm parallel plate geometry, generally following the procedures in ASTM D7175, *Determining the Rheological Properties of Asphalt Binder Using a Dynamic Shear Rheometer*. The data from each of these experiments were then combined to form a master-curve of stiffness/modulus over a complex modulus (G^*) range from 100 Pa to 100 MPa. Test temperatures generally ranged from -40 to +150°C, with slight variations depending on the stiffness of the materials. A frequency sweep was conducted at each temperature using eleven frequencies from 0.1 to 10 rad/s, inclusive, spaced logarithmically. The applied shear strain varied depending on the test temperatures and geometry. At very low temperatures using the 4-mm parallel plate geometry, the applied shear strain was 0.05%. An applied shear strain of 0.2% was used with the intermediate test temperatures and the 8-mm geometry. An applied shear strain of 0.3 to 0.5% was used for testing conducted at high temperatures with the 25-mm parallel plate geometry. A typical example of the data collected is presented in Figure 5. The data were then used within the RHEA software to generate master-curves of stiffness, as shown in Figure 6.

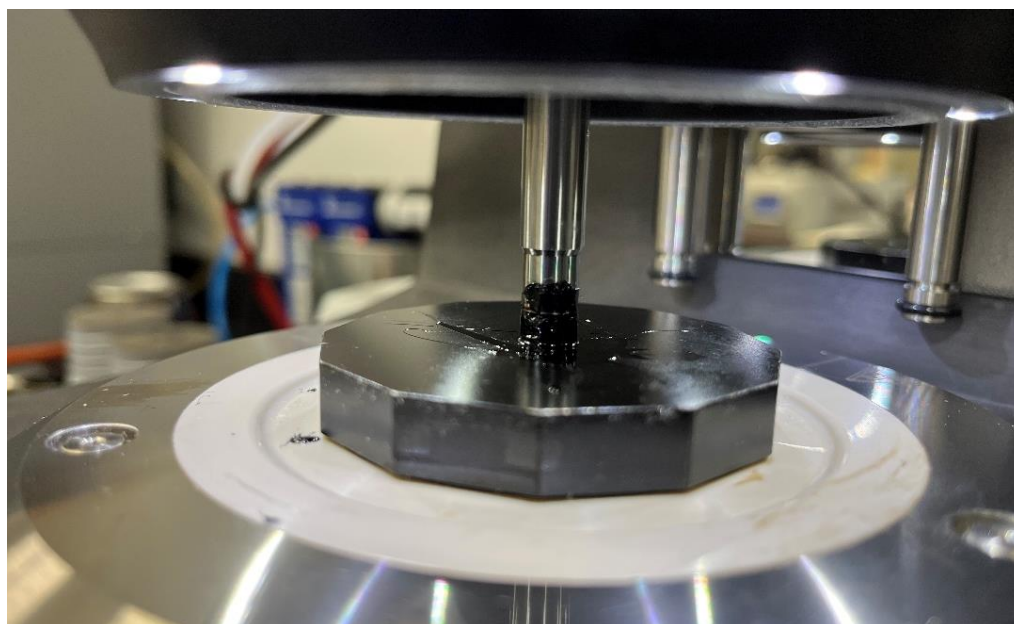


Figure 4: DSR Testing Using the 8-mm Parallel Plate Measurement Geometry

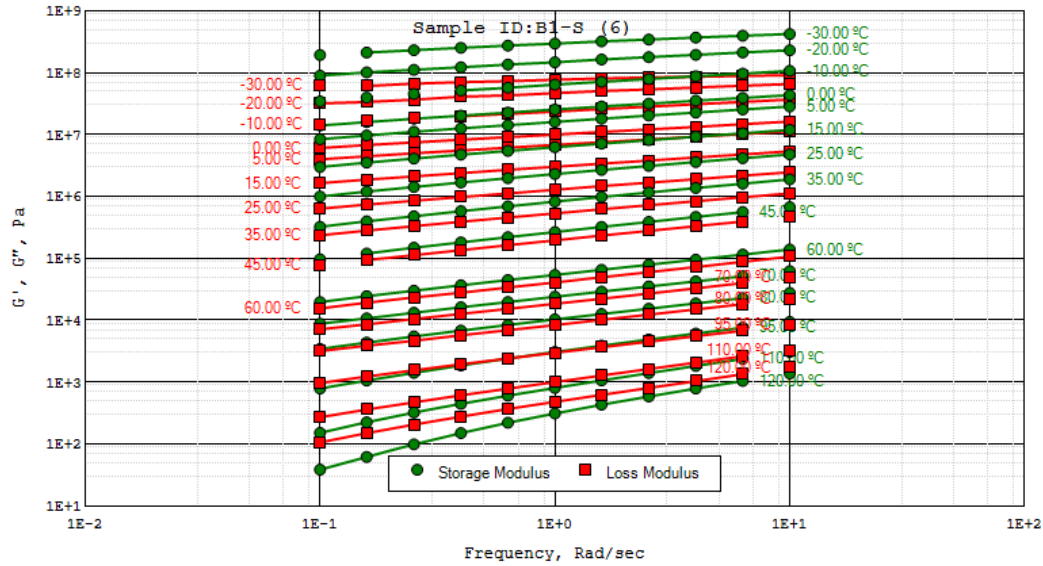


Figure 5: Isotherms of Stiffness for Sample B1-S (6) Collected from DSR Testing

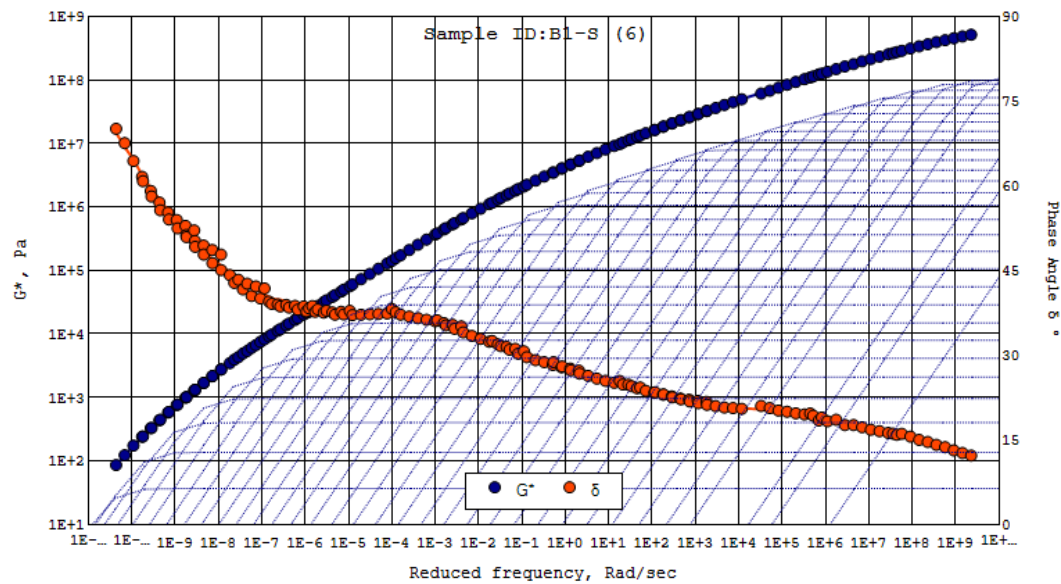


Figure 6: Master-curve of G^* and Phase Angle (δ) for Sample B1-S (6)

Bending Beam Rheometer

ASTM D6648, *Determining the Flexural Creep Stiffness of Asphalt Binder Using the Bending Beam Rheometer (BBR)*, was followed when conducting the Bending Beam Rheometer (BBR) testing. BBR equipment is shown in Figure 7.



Figure 7: Bending Beam Rheometer (BBR) Test Equipment

This testing was conducted on two box samples and one sample from an exposed shingle. The pouring of the beams from the recovered asphalt was found to be more difficult than has been experienced with paving grade asphalt binders due to the higher stiffness of the recovered shingle binder. Two test temperatures were used (-10 and -20°C) for three of the data sets, whereas four temperatures (-30, -20, -15 and -10°C) were used for the data set generated for Sample B1-B (1). A typical result is shown below in Figure 8. In this temperature range the stiffness varied from 22 MPa to 427 MPa (36 to 284 MPa at 60 seconds loading time). This stiffness is relatively low at these temperatures when compared to paving grade asphalt binders. Thus, while the material was stiffer at the preparation temperatures it was less stiff than typical paving grade asphalt binders when tested under creep loading. This response is a consequence of the lower temperature susceptibility of asphalt roofing grades. Master-curves of stiffness were produced for the data sets, and these are shown in Figure 9.

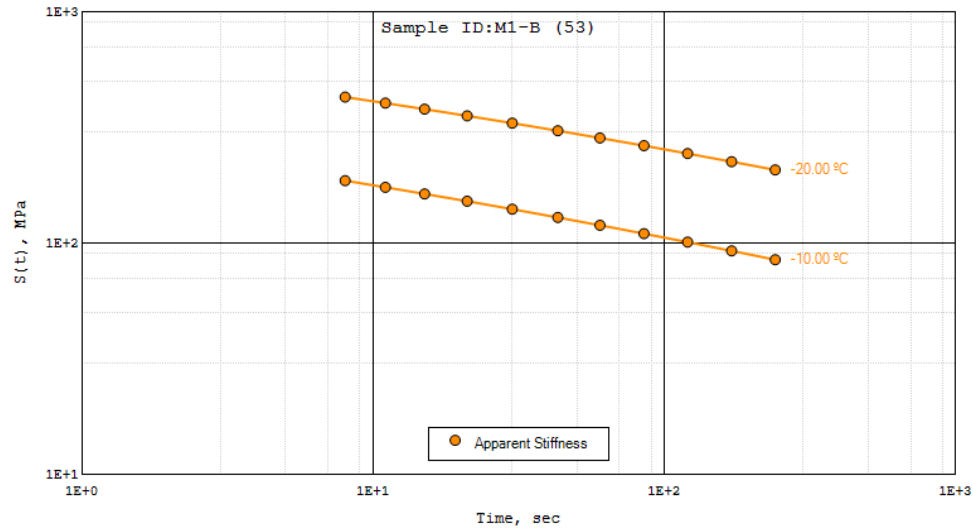


Figure 8: Typical BBR Isotherms from Testing at Two Temperatures, -10 and -20°C

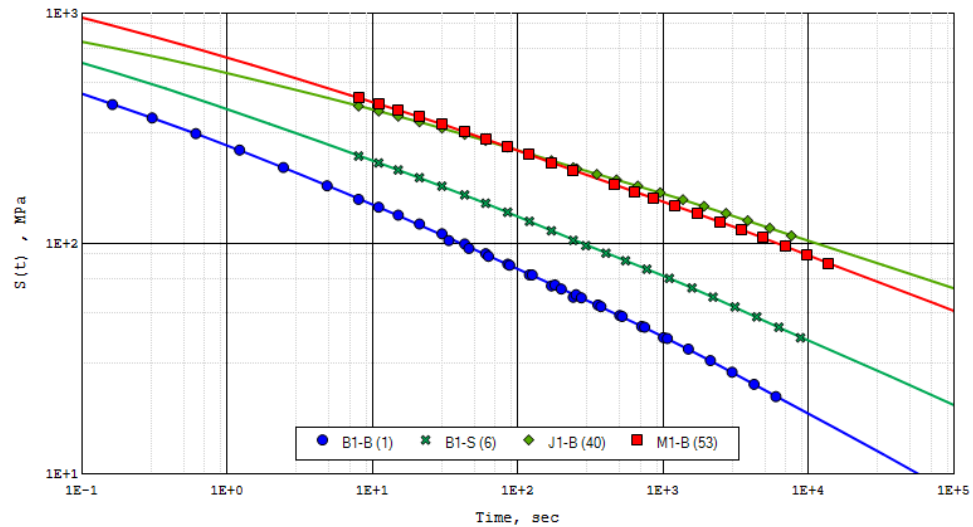


Figure 9: Master-curves of Stiffness at a Reference Temperature (T_{ref}) of -20°C

The data from the BBR were then converted to dynamic format using a fit of the retardation spectra to the compliance master-curve, $D(t)$, using an assumed value of 0.5 for Poisson's ratio. The corresponding frequency to loading time was determined as ω (radians/second) = 1/seconds. A reverse shift was then applied to develop isotherms that correspond to the original BBR test data. An example of the resulting isotherms is shown below for the material referenced as B1-B (1) in Figure 10.

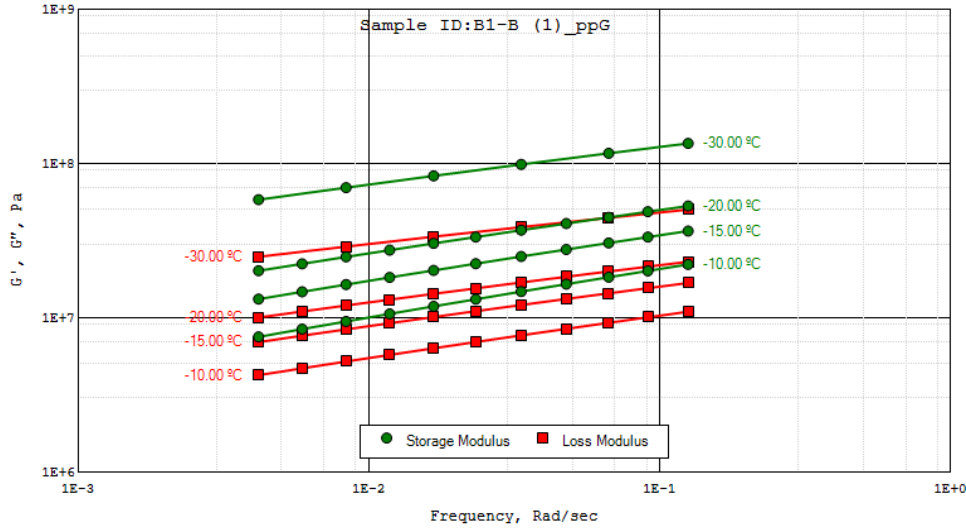


Figure 10: Isotherms of G' and G'' Computed from BBR Data Obtained for Sample B1-B (1)

Combination of Data using RHEA

Data from the BBR and DSR were reviewed to determine if they could be combined into a single master-curve. An example of these data is given for Sample B1-B (1) in Figure 11. This example shows a good match between the two data sets – but, in general, the research team found that the comparison was a little poorer than this (Note: it may be difficult to see, but in Figure 11 the BBR data, shown in blue, is overlaid by the DSR data, shown in red, in the region of G^* from $1E+7$ to $1E+9$ Pa.). The practical implication of the data shown in Figure 11 is the observation that the BBR testing does not offer any additional information on low temperature stiffness compared to what could be obtained with the DSR. Given that material quantities were limited, the research team limited use of the BBR to just the four samples – B1-B (1), B1-S (6), J1-B (40), and M1-B (53).

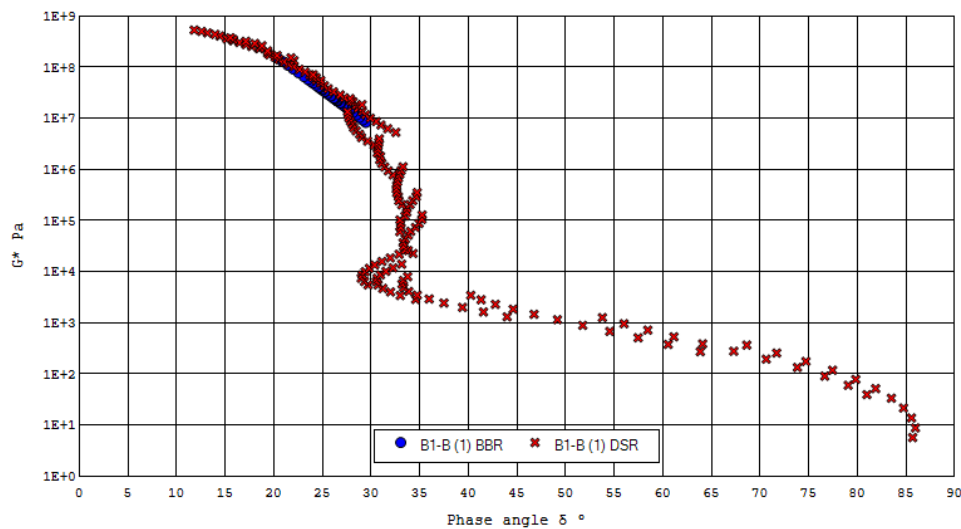


Figure 11: Black Space Comparison of DSR and BBR Data Sets

Ultimate Tests

The use of ultimate tests that consider the stress, strain and/or energy to a defined failure condition is considered important for modified binder systems to classify their performance attributes. In this initial study several ultimate tests were explored to assess the performance of materials at a cracking/fracture condition. Previous work conducted with paving grade asphalt binders suggests that cracking occurs when the stiffness is greater than approximately 1 MPa. Anderson et al. (2001) presented research showing that “true fatigue” for asphalt binders generally occurred at stiffness (G^*) values above 5 to 18 MPa ($5E+6$ to $1.8E+7$ Pa), whereas the term “instability flow” was associated with failure that exhibited large deformations below this stiffness level. This principle is consistent with brittle-to-ductile behavior that can be observed with direct tension test data (Rowe and Sharrock, 2004). In the work by Rowe and Sharrock, the peak energy associated with fracture was considered to occur when the relaxation modulus $E(t)$ was approximately 20 MPa – consistent with the range that the transition from instability flow to true fatigue occurred in the work conducted by Anderson et al. (2001). In the research conducted by Anderson et al., the maximum fatigue life occurred at this transition point, which using Rowe and Sharrock’s work, is consistent with the maximum toughness (defined here as the area under a stress-strain curve). Consequently, it was decided that ultimate properties should be evaluated in the stiffness range where G^* is approximately 5 MPa and higher.

While these tests can involve stress and strain magnitudes that are greater than those associated with master-curve development and beyond the linear range of behavior, it has been shown that the stiffness from these types of measurements can be used to normalize the data into ultimate property master-curves (Rowe and Sharrock, 2024). The work with test methods used for measuring ultimate properties is described in the following sections.

Asphalt Binder Cracking Device (ABCD)

This test procedure (AASHTO T387, 2022) is used to determine the thermal cracking temperature of an asphalt binder. The device uses a strain gauge inserted within a ring of asphalt binder to measure thermal strain (ϵ) as the binder is cooled at a controlled rate within an environmental chamber (Figure 12 and Figure 13).

Each ABCD ring is connected to a data acquisition system. As the specimen cools, thermal stresses begin to accumulate within the binder, resulting in a rupture (crack) at the point when accumulated stresses exceed binder strength. This is noted by a “jump” in strain on the plot of temperature and microstrain ($\mu\epsilon$) as shown in Figure 14. Cracking temperature and strain jump are reported, as well the fracture stress at the cracking temperature (σ_{AC}).

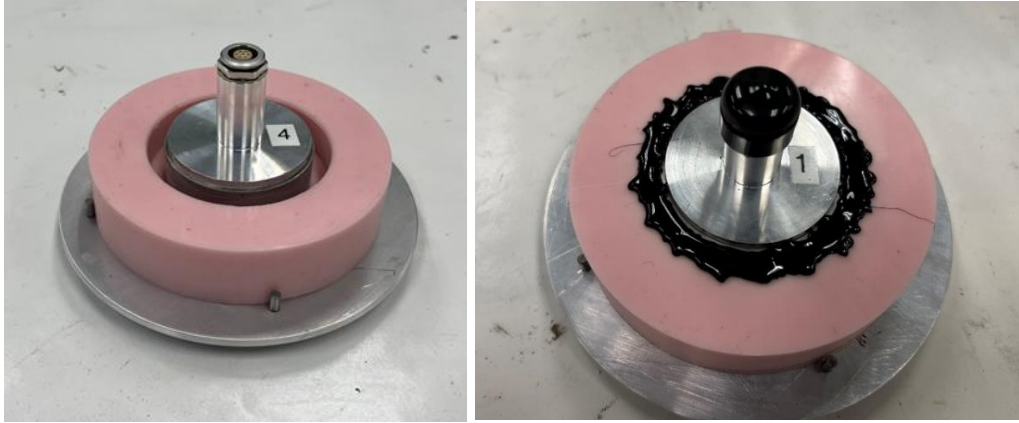


Figure 12: ABCD Ring and Mold – Unfilled (left) and Filled with a Sample (right)



Figure 13: ABCD Specimens in Environmental Chamber

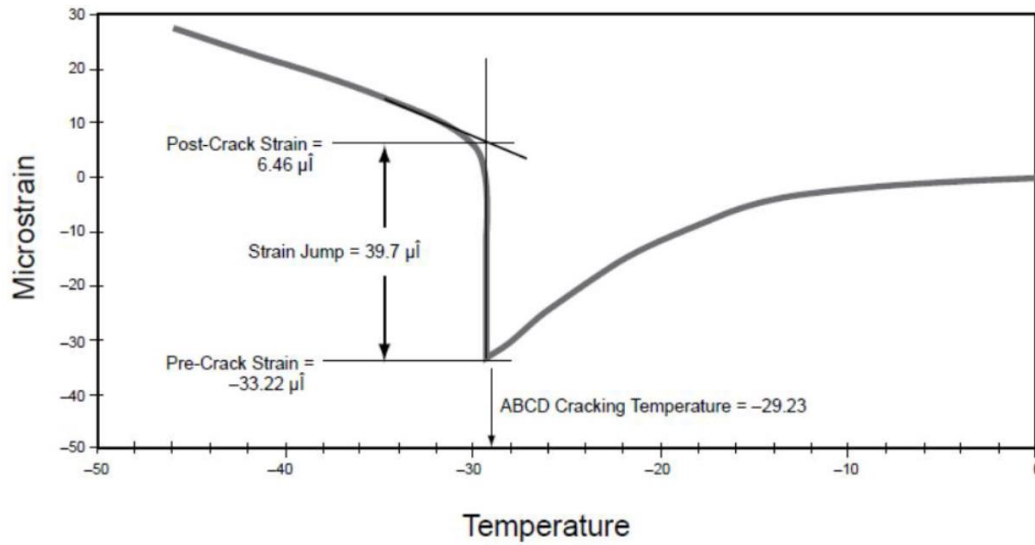


Figure 14: Typical Strain vs. Temperature Plot for ABCD Test (from AASHTO T387)

Simplified Double-Edge-Notched Tension (SDENT) Test

The SDENT test is a modified version of the standard DENT procedure (provisional standard AASHTO TP 113, 2022). Per AASHTO TP 113, the DENT test is used to measure a binder's resistance to ductile failure by placing asphalt binder specimens with varied ligament lengths (l) in tension until rupture occurs. Displacement (d) is measured electronically, and tensile load (P) is measured via a load cell. The total work of failure (W_t) calculated as the area under the curve from a plot of displacement and tensile load. Additionally, specific total work of failure (w_t) is calculated as a function of specimen dimensions and is plotted against ligament length to find essential work of failure (w_e). Other parameters are calculated as well but are not relevant to the purposes of this report.

A simplified version of this procedure (SDENT) is outlined by Christensen and Tran in NCHRP Report 982, *Relationships Between the Fatigue Properties of Asphalt Binders and the Fatigue Performance of Asphalt Mixtures*, as a means of evaluating the strain capacity of an asphalt binder. Per this simplified method, the DENT procedure is performed at a single ligament length of 5 mm (Figure 15) to obtain W_t through plotting load and displacement as shown in Figure 16.



Figure 15: Molded SDENT Specimens (5-mm Ligament Length)

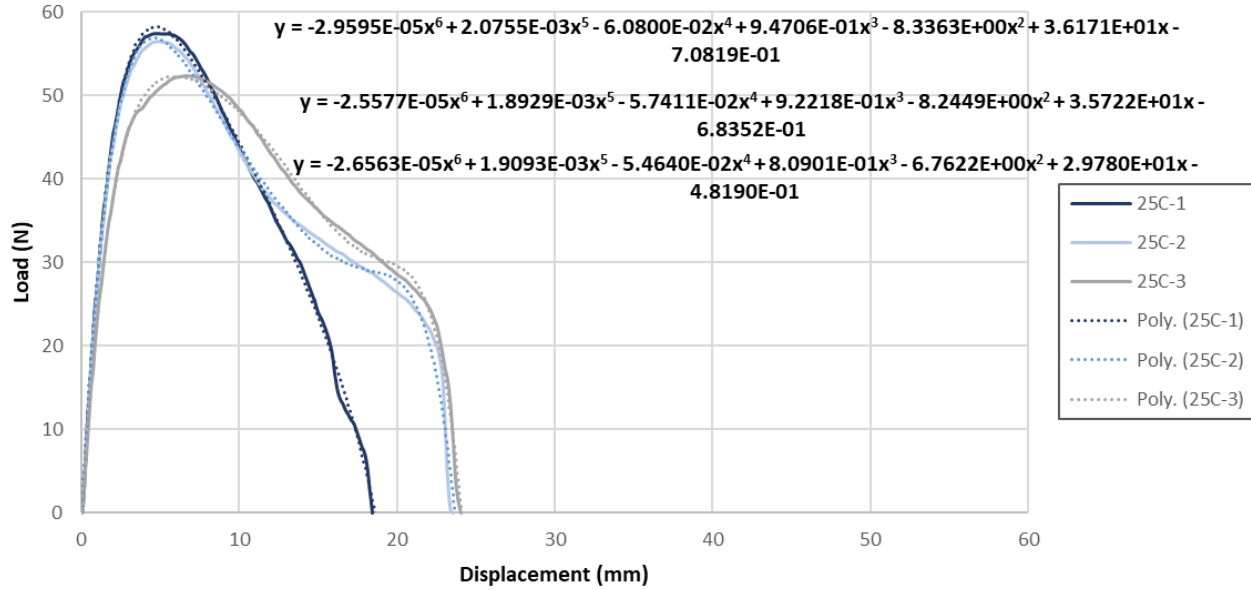


Figure 16: Typical Load vs. Displacement Plot for SDENT Test at 25°C

Further analysis is performed to find the fatigue/fracture performance ratio (FFPR), defined in NCHRP Report 982 (Christensen and Tran, 2022) as “the ratio of the strain capacity of a given binder to the average or typical strain capacity”, and calculated by the equation:

$$FFPR = \frac{Extension}{48S^{-0.371}}$$

where:

Extension = displacement to a defined point¹

S = Initial stiffness – secant modulus at a loading time of three seconds

In this study, SDENT was performed at 10°C, 15°C, 20°C, and 25°C to target the expected transition region from ductile to brittle behavior.

Binder Yield Energy Test (BYET)

The Binder Yield Energy Test (BYET) measures the required energy needed to cause an asphalt binder to yield when subjected to a monotonically applied shear stress. It is performed on the DSR by applying a constant shear strain rate to the binder at 1%/second until a peak stress is observed. Binder yield energy (BYE) is determined by finding the area under the stress-strain curve to the point of maximum stress, Figure 17. Details on the procedure are given in AASHTO TP123, *Measuring Asphalt Binder Yield Energy and Elastic Recovery Using the Dynamic Shear Rheometer*.

¹ Defined points included in this study were extension to 20% of peak load (E_{20}) and total extension to failure (E_{TEF}). This location was taken after the peak load was obtained using a polynomial fit to the data.

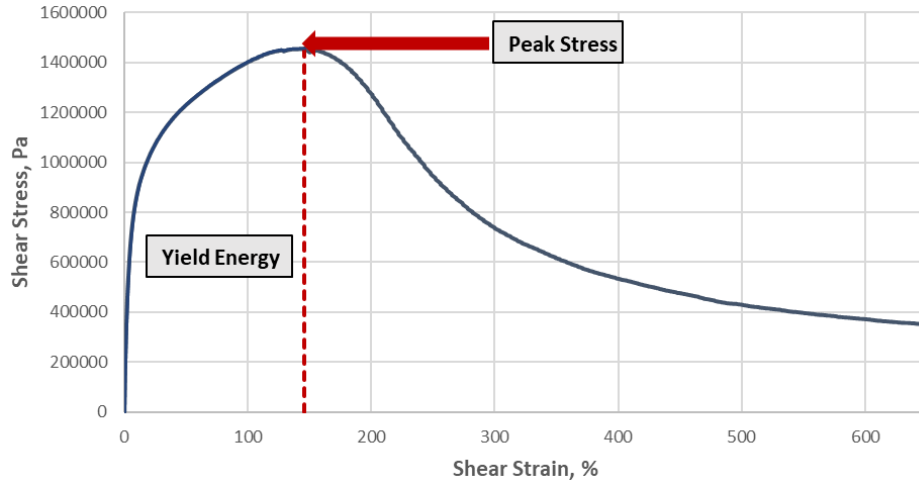


Figure 17: Typical Stress-Strain Curve for BYET

Initial efforts in performing the BYET procedure on trial roofing materials at multiple test temperatures produced mixed results, in part due to the difficulty of maintaining proper sample adhesion when applying high strains at lower temperatures. Figure 18 and Figure 19 show trial runs on two standard shingles.

Due to the adhesive issues, erratic curves and lack of clear peak stress that were noted in the initial trials, a modified BYET procedure was developed. A detailed outline of this procedure can be found in Appendix A, but the main procedural alterations are as follows:

1. An extended adhesion soak (preconditioning) time at an elevated temperature (10 minutes at approximately 90-120°C)
2. A slower cooling rate from loading temperature to test temperature ($6 \pm 1^\circ\text{C}/\text{minute}$)
3. A normal force control procedure during adhesion soak and cooling
4. Slower loading rate of 0.05 RPM (approx. 0.005rad/s)
5. Smaller test gap (1.70 mm)

Materials were tested at two temperatures using the modified BYET procedure: at an equal-stiffness temperature (where $G^*_{10\text{rad/s}}$ was 10 MPa), and at 20°C.

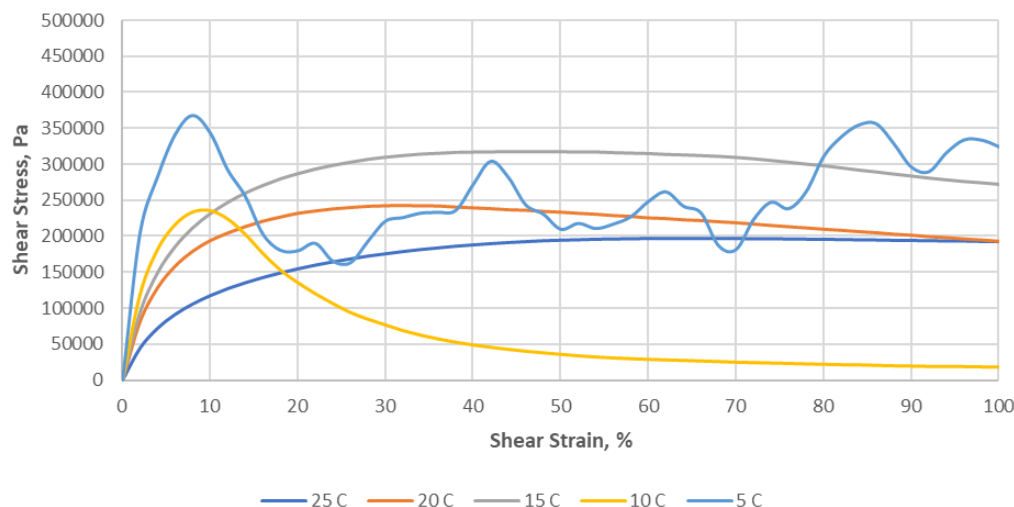


Figure 18: BYET – Roofing Trial Run #1

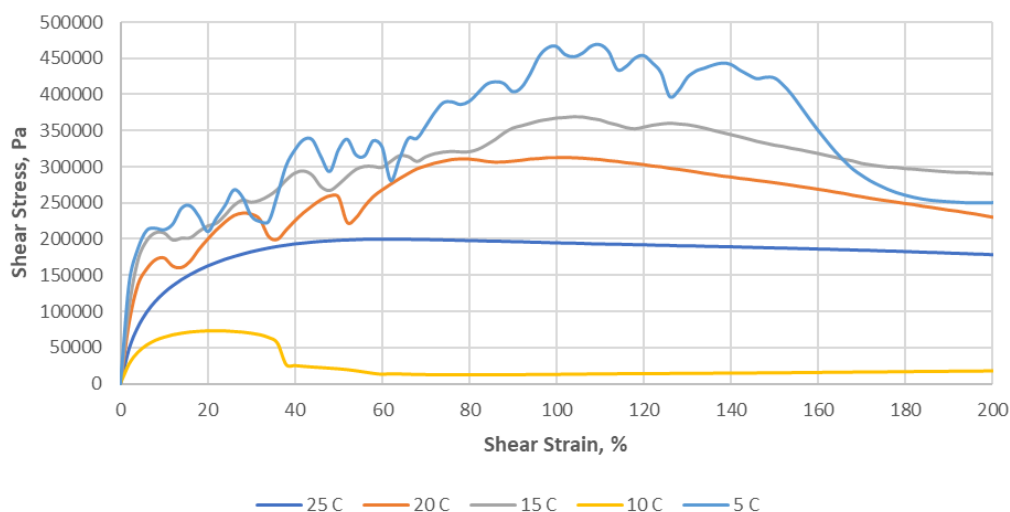


Figure 19: BYET – Roofing Trial Run #2

Poker Chip Test

The Poker Chip test measures² the force and ductility of an asphalt binder under a constant load rate application test, with a specimen configuration similar to that of a poker chip –specifically, with a specimen dimension that is 57.15 mm in diameter and 1.5875 mm in thickness and made with 4.5+/- 0.05 grams of asphalt binder. The top plate, which adheres to the sample, has a diameter of 50.8mm. At the required test temperature, the top plate is moved vertically while maintaining a monotonically increasing load at a rate of 2 N/s.

Most of the testing conducted in the USA to date has been carried out at room temperature (~25°C). However, in this research tests were conducted from 0 to 30°C to investigate if the method can be used to

² Testing was performed by Prof. Ramex M. Hajj, University of Illinois at Urbana-Champaign, 1210 Newmark Civil Engineering Lab, 205 N Mathews Ave., Urbana, IL 61801 | rhajj@illinois.edu | (217) 244-6107

define the brittle-to-ductile flow/fracture behavior of the shingle asphalt binders. As this work was started, the research team hypothesized that the transition from ductile/flow to brittle behavior over that temperature range would be strongly correlated to the binder stiffness, expressed as a relaxation modulus. This would allow for a ranking of the various shingle asphalt binders in the study.

In review of published data, it was observed that binder rheological properties can be strongly correlated to data from the Poker Chip test, thus making this a viable candidate tool for assessment of the performance of ultimate properties (Figure 20).

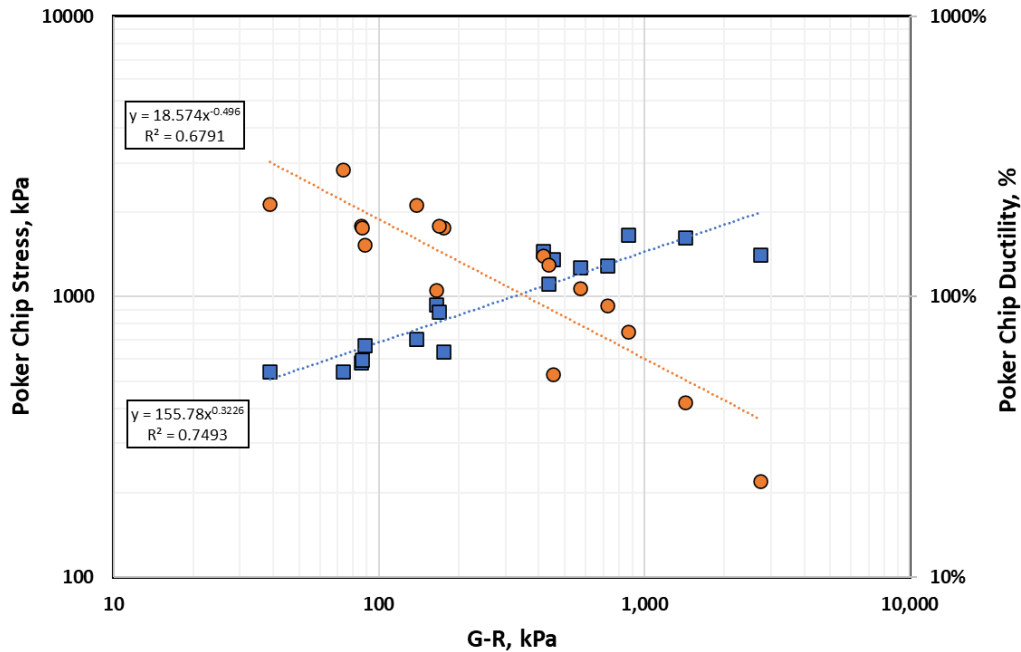


Figure 20: G-R Binder Parameter vs. Poker Chip Stress and Ductility (after Filonzi et. al., 2022)

Initially, an evaluation of the Poker Chip test method for roofing grade binders was conducted with a “trial binder” recovered from the commercial shingle purchased at a local hardware store. This was followed by testing select binders recovered from the State Farm aging farm. Poker Chip testing was discontinued after a few materials, as discussed later in this report.

Rheological Analysis

A previous section of this report showed some of the data collected during the testing process. The materials evaluated include harvested samples from the TRAIL aging farm with different exposures as well as their corresponding “unaged” samples stored in boxes. Although not vacuum sealed, the box samples were stored, unopened, in a space with a controlled environment and were considered as having aged to a minimal extent. In the rheological testing, it was apparent that the materials in more extreme exposures aged more significantly. The comparisons are shown as follows:

- **Material B1** - BBR stiffness of material B1-S (6), from an aged shingle with a southern exposure, shows a higher stiffness compared to the box sample of the same material, Sample B1-B (1), as shown in Figure 21. DSR data is shown in Figure 22 and Figure 23 for B1 southern exposure and box sample. Figure 22 shows how the stiffness has increased at a reference temperature of 25°C. The plot in Figure 23 shows the Black space plot. In this Figure, it can be seen that the phase angle has reduced at higher stiffness, whereas at intermediate stiffness values the phase angle has increased. This type of behavior with aging is typical of changes seen in polymer modified binders.
- **Material G1** - DSR data are shown in Figure 24 and Figure 25 for Sample G1, representing the box sample (unaged) and aged shingles with both southern and northern exposures. Figure 24 shows how the stiffness has increased with aging at a reference temperature of 25°C. It also shows that the curve for the Northern exposure lies clearly in between the curves for the box sample and the Southern exposure, indicating less aging on the northern-facing side of the test roof, as expected. The plot in Figure 25 shows the Black space plot which again indicates use of a modified binder. In this plot the rheology at the higher stiffness is very consistent and the only phase angle changes occur at the low stiffness values. This could be a result of some polymer degradation at these low stiffness values.
- **Material J1** - DSR data for Sample J1 is shown in Figure 26 and Figure 27. The rheology is typical of a non-modified oxidized roofing grade binder. The southern exposure results are indicative of a greater degree of aging.
- **Material M1** - Material M1 (Figure 28 and Figure 29) shows similar performance to Material J1. A box sample tested for this material showed lower stiffness, which is consistent with less aging.

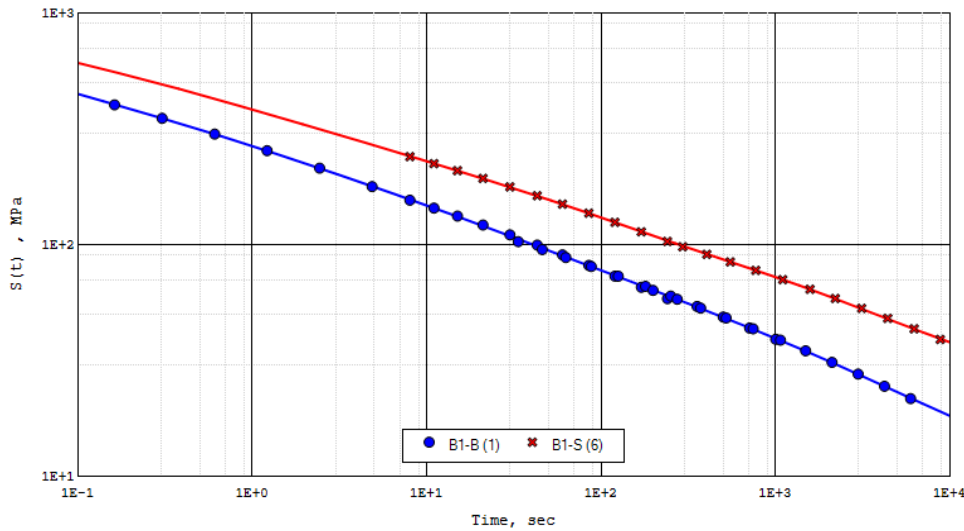


Figure 21: BBR Stiffness of Sample B1 - Southern (S) Exposure versus Box (B) - at a Reference Temperature (T_{ref}) of -20°C

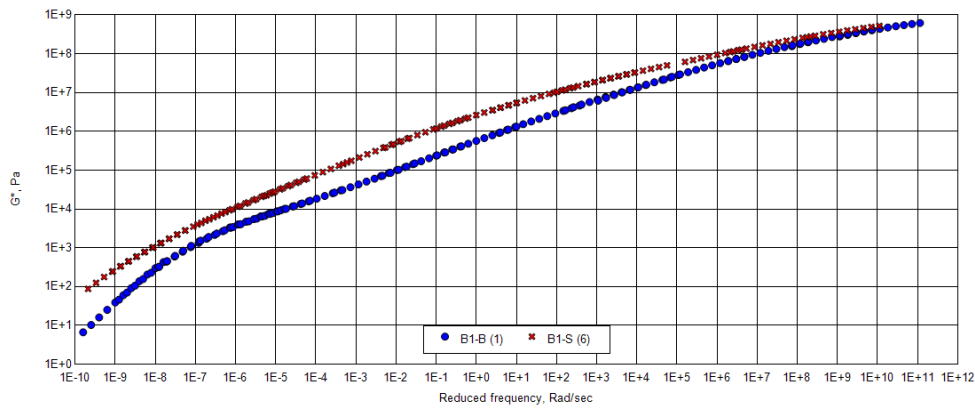


Figure 22: DSR Master-curve of Sample B1 - Southern (S) Exposure versus Box (B) - G^* versus Reduced Frequency at a Reference Temperature (T_{ref}) of 25°C

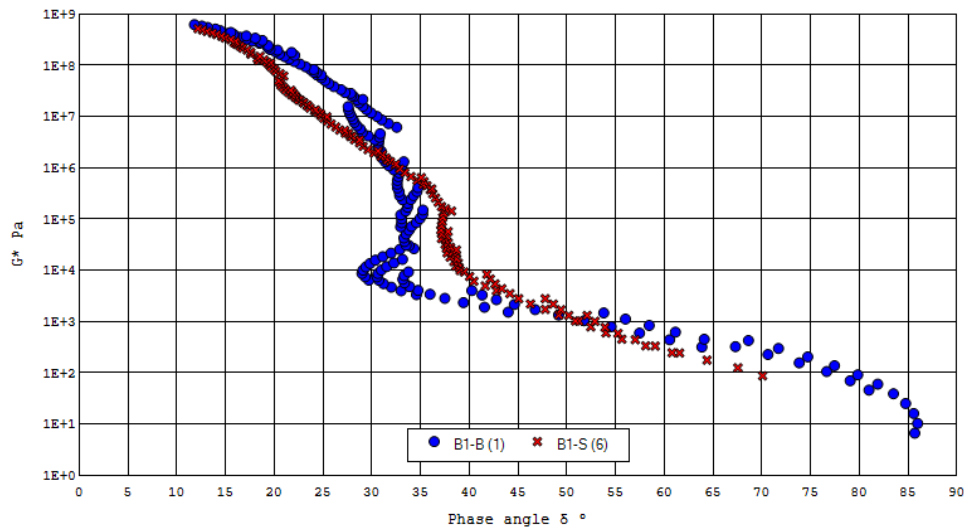


Figure 23: Black Space Plot for Sample B1 – Southern Exposure (S) versus Box (B)

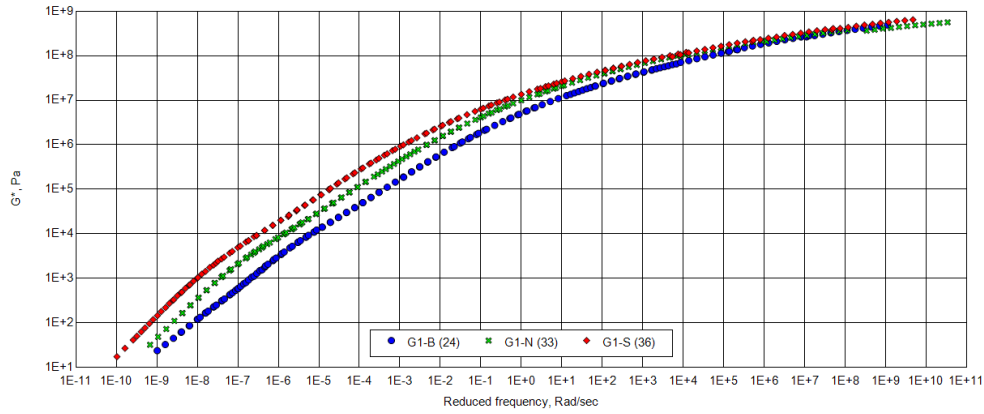


Figure 24: DSR Master-curve of Sample G1 - Southern (S) Exposure, Northern Exposure (N), and Box (B) - G^* versus Reduced Frequency at a Reference Temperature (T_{ref}) of 25°C

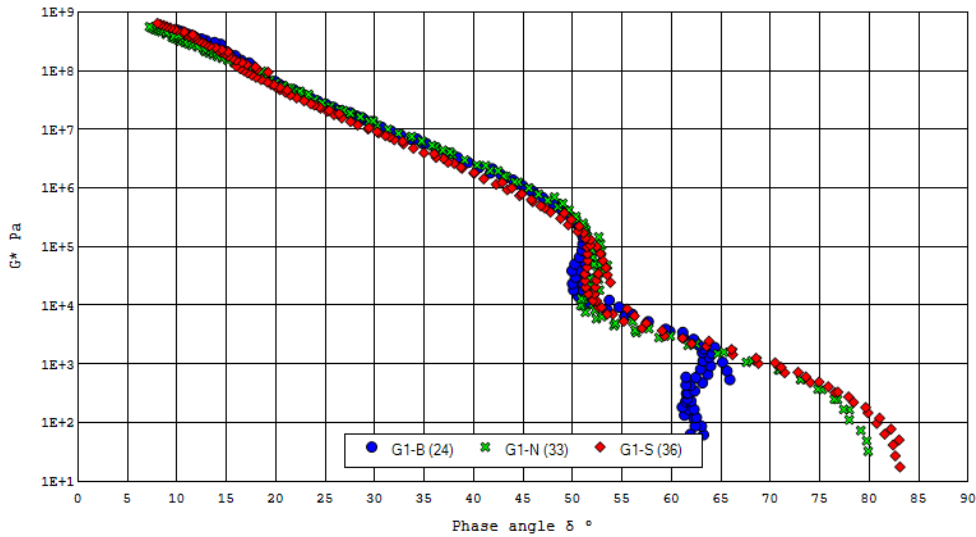


Figure 25: Black Space Plot for Sample G1 – Southern Exposure (S), Northern Exposure (N), and Box (B)

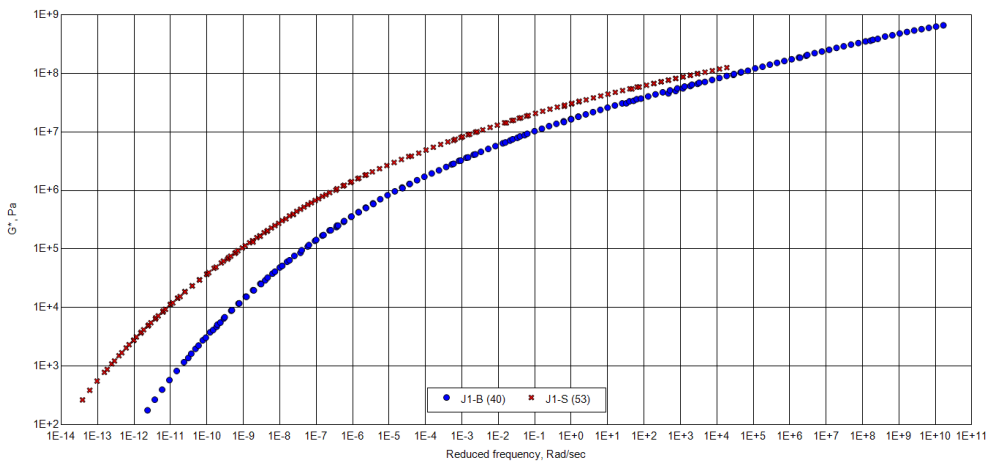


Figure 26: DSR Master-curve of Sample J1 - Southern (S) Exposure versus Box (B) - G^* versus Reduced Frequency at a Reference Temperature (T_{ref}) of 25°C

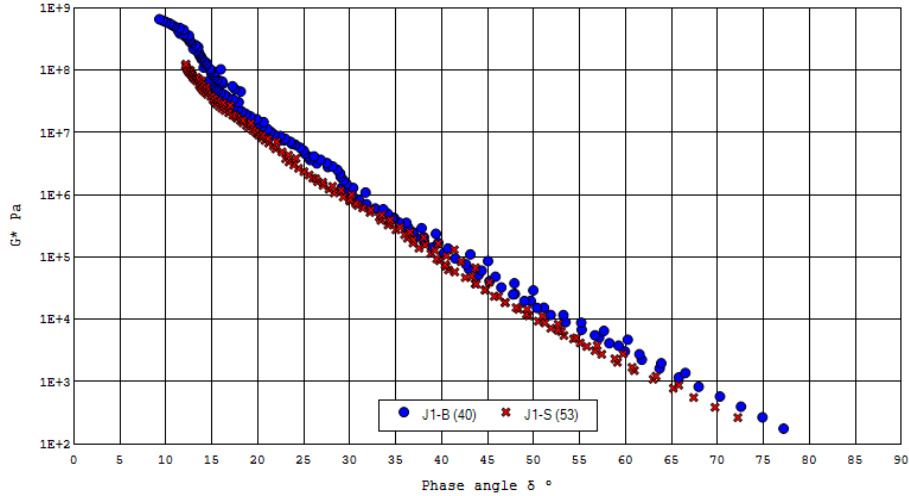


Figure 27: Black Space Plot for Sample J1 – Southern Exposure (S) versus Box (B)

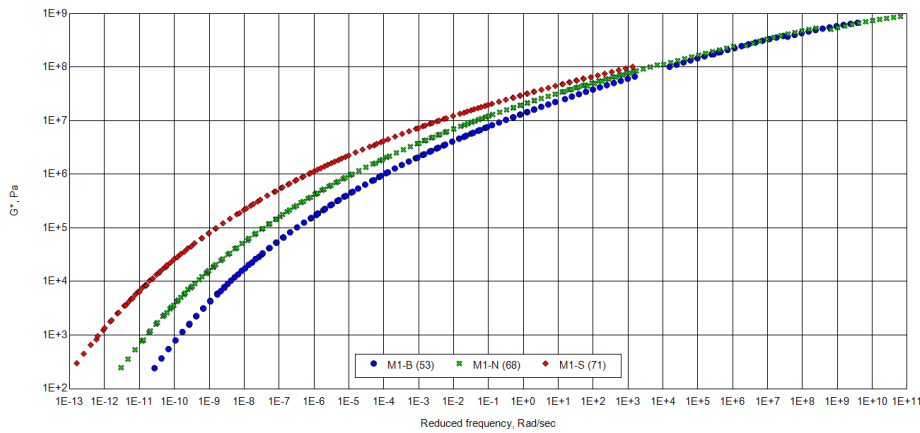


Figure 28: DSR Master-curve of Sample M1 - Southern (S) Exposure, Northern Exposure (N), and Box (B) - G^* versus Reduced Frequency at a Reference Temperature (T_{ref}) of 25°C

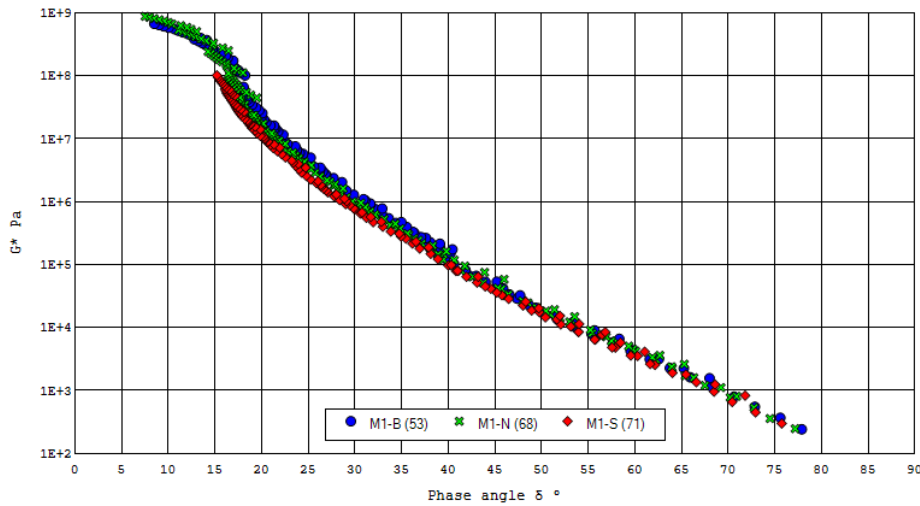


Figure 29: Black Space Plot for Sample M1 – Southern Exposure (S), Northern Exposure (N), and Box (B)

Parametric Analysis

Rheological Parameters

The shape of a master-curve in the higher stiffness region can typically be defined by one of four parameters. These are:

- 1) ΔT_c from BBR analysis,
- 2) R-value from a fit of the data to the Christensen-Anderson model (or via simplifications and closed form solutions),
- 3) the phase angle, δ , at a given stiffness value, and/or
- 4) the logarithm of the cross-over modulus, G_c (i.e. the modulus where phase angle is 45°).

In this work, the first two methods were not found to be suitable for evaluating the roofing asphalt binder samples. The use of the ΔT_c from BBR analysis is problematic since forming the beams for aged roofing materials was difficult. Additionally, the temperature susceptibility of the samples resulted in many isotherms being needed to obtain this parameter. For instance, four isotherms were obtained for Sample B1, but the information was still insufficient to enable proper computation of ΔT_c without extrapolation. The use of the rheological index (R-value) was not possible since the fit of the data to the Christensen-Anderson model was generally poor, with an RMS error greater than 2.5%. The R-value can also be determined via the use of a single value of complex modulus and phase angle as discussed by Anderson et al. (2011). However, the simplifications to the approach using single values of phase angle and stiffness will theoretically result in a poorer estimation than using one of the other two methods, in part because the simplification requires the use of an assumed glassy modulus (G_g) of 1000 MPa (Rowe et al., 2023). Thus, the two methods used in this work were the logarithm of the cross-over modulus ($\log G_c$) and phase angle at a given modulus value (Kriz, 2020). Each of these methods effectively define the shape of the master-curve in the higher stiffness region in a similar manner to the R-value.

The value of G^* (stiffness) used for the phase angle calculation is 10 MPa. This stiffness was chosen for several reasons:

1. It is a stiffness that can be consistently obtained from DSR measurements using 8-mm parallel plate geometry, thus avoiding issues experienced with testing using either the BBR or DSR with 4-mm parallel plate geometry.
2. It is similar to the value proposed by Pavel Kriz for paving grade binders – 8.967 MPa. (Kriz et al., 2020).
3. It is the same value of stiffness used by the FAA in recent work, in which they use the tangent of phase angle at a complex shear modulus value (G^*) of 10 MPa (Bennert, et al., 2022)
4. It appears to be a good descriptor of the shape of the master-curve in the high stiffness region, related to the relaxation properties.

Thus, a reasonable body of work will be available on binders at this value of stiffness ($G^*=10$ MPa) which can support the work of this research. Furthermore, if the temperature is obtained (at a fixed frequency) corresponding to this stiffness value ($T_{G^*=10 \text{ MPa}}$), a measure of the hardness of the binder can be determined. Higher temperatures for $T_{G^*=10 \text{ MPa}}$ correspond to stiffer binders.

The shape of the master-curves and the modification types used reveal that, for certain binders, a relationship exists between two common ways of defining the shape of the master-curve in the higher

stiffness region (Figure 30). However, with certain modification systems, the retention of stiffness caused by the polymer network occurs in a different stiffness region of the master-curve, resulting in the atypical behavior as shown by material B1. For typical paving-grade binders, a good correlation will exist for cross-over modulus and phase angle at 10 MPa. However, for roofing materials, such as Material B1, the cross-over modulus occurs in a stiffness region much lower than the range typically associated with cracking/toughness properties.

Two of the four types of shingles used in this research, Materials B1 and G1, contained polymer-modified binders. The Black space plot contrasts the box (B) samples of these two materials in Figure 31. The higher phase angle at the value of G^* around $1E+8$ Pa suggests that the base binder used to produce Sample B1-B may have been softer than the base binder used to produce Sample G1-B. However, the polymer modification used in Material G1 results in a higher phase angle in the stiffness (G^*) range of $1E+4$ to $1E+7$, which implies that the polymer modification allows greater relaxation to occur in this intermediate stiffness region. Both materials exhibit properties close to a viscoelastic solid while transitioning to a viscoelastic liquid behavior at a certain temperature. This transition can be observed by inspection of the isochronal data for phase angle (at 10 rads/sec loading frequency), as shown in Figure 32, which suggests a changeover occurring at approximately 60 to 80°C for both materials.

It is important to observe that the G_c value for Material B1 may not be related to cracking since the stiffness is significantly below the range where cracking/toughness issues affect performance.

Since the use of properties in the cross-over region (where the phase angle is 45°) is problematic, the research team chose to evaluate the modulus and temperature associated with a phase angle (δ) of 27 degrees. This phase angle is consistent with the m-value from a bending beam rheometer test being approximately equal to 0.300 (Rowe, 2014). In a similar manner to cross-over temperature (denoted as T_{G_c}), the $T_{\delta=27^\circ C}$ can provide an indication of the relative hardness/stiffness of the product being used.

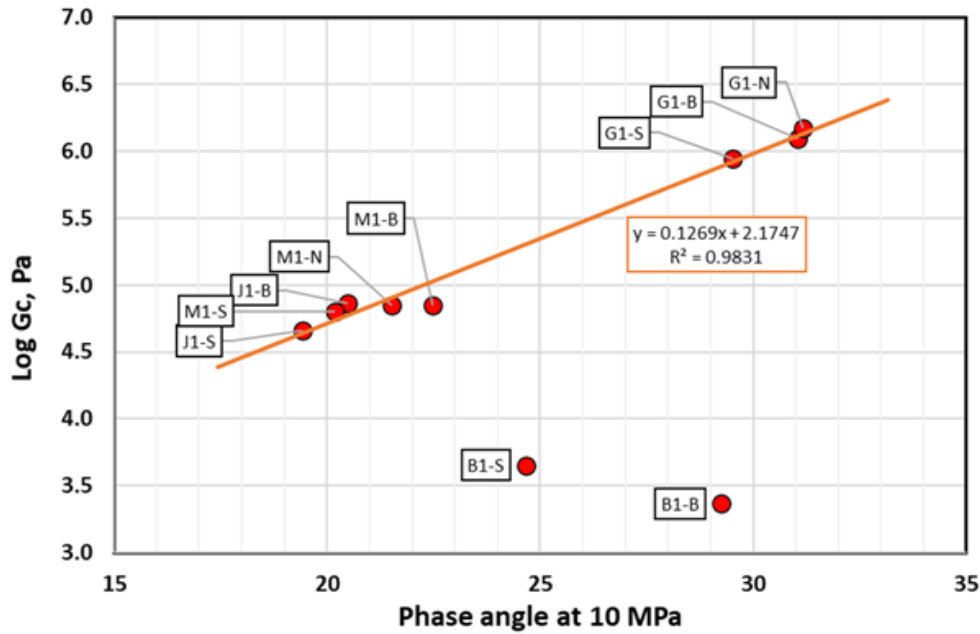


Figure 30: Relationship between Two Measures of Master-curve Shape – Phase Angle at Constant Modulus and Log of the Cross-over Modulus (Log G_c)

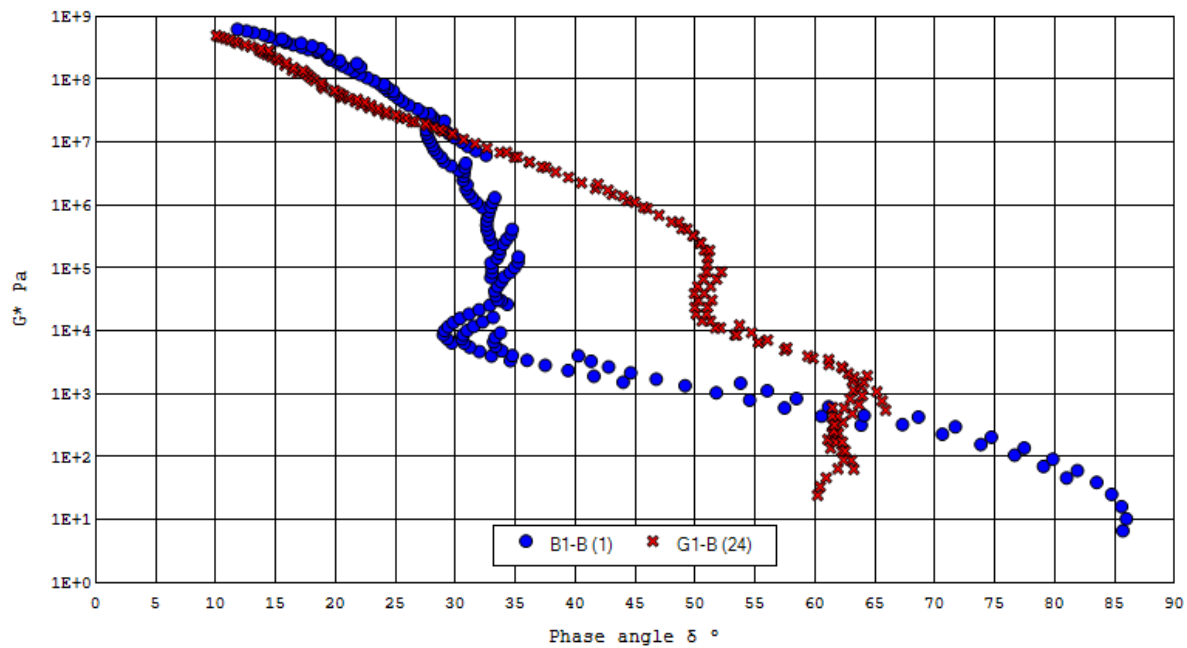


Figure 31: Black Space Plot for Materials B1-B (1) and G1-B (24)

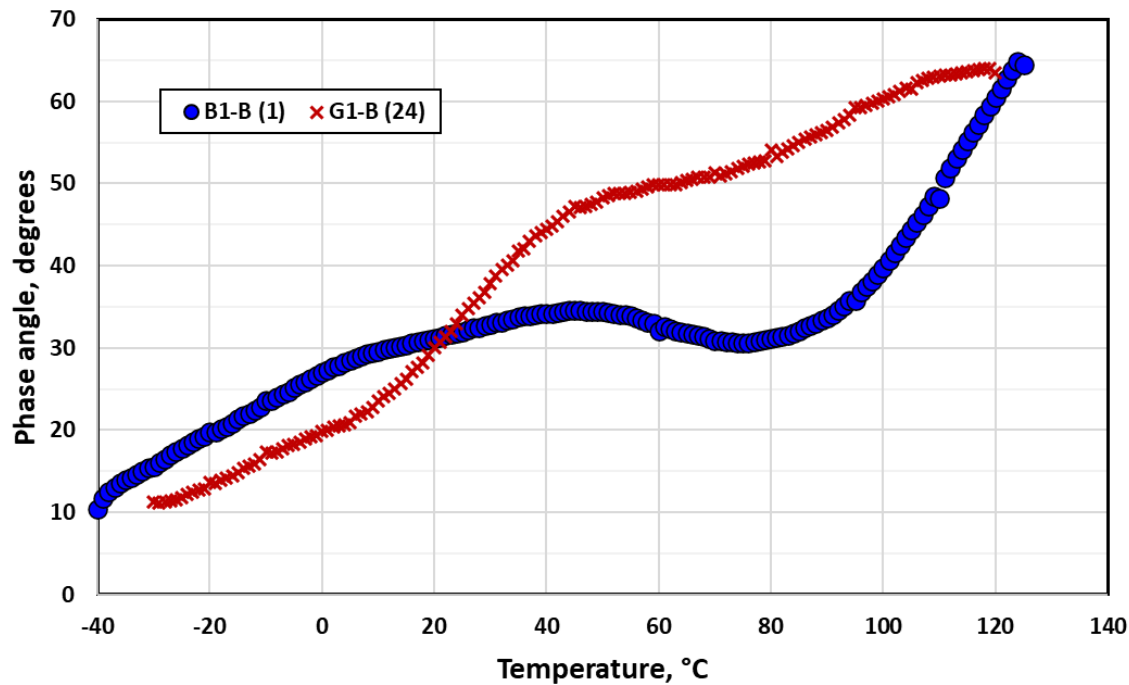


Figure 32: Isochronal (10 radians/second) Curves for Phase Angle as a Function of Temperature – Materials B1-B (1) and G1-B (24)

As a material ages, a typical response exhibits a decrease in the phase angle and the cross-over modulus, G_c , compared to the unaged or less-aged conditions. The data shown in Table 3 indicates that the expected trend is more evident in phase angle results than for $\log G_c$. For B1, $\log G_c$ shows an atypical (opposite) trend. For Materials G1 and M1, there is no discernible trend.

Table 3: Analysis Parameters Determined from Master-curves

Material	Exposure	Sample	Error, rms%	T_{10MPa} , °C	δ_{10MPa} , degrees	G_c , Pa	$\log G_c$	T_{G_c} , °C	$T_{\delta=27^\circ C}$, °C
B1	B	1	1.8	7.8	29.2	2.33E+03	3.37	105.2	0.3
B1	S	6	0.9	18.1	24.7	4.49E+03	3.65	108.7	25.1
G1	B	24	2.6	21.8	31.0	1.24E+06	6.09	40.6	15.3
G1	N	38	1.9	27.8	31.2	1.49E+06	6.17	44.9	21.2
G1	S	36	2.0	31.4	29.5	8.79E+05	5.94	54.8	27.1
J1	B	40	1.6	34.3	20.5	7.32E+04	4.86	95.9	56.5
J1	S	53	1.3	46.1	19.4	4.62E+04	4.66	119.9	72.1
M1	B	53	1.1	32.3	22.5	7.02E+04	4.85	96.8	49.2
M1	N	68	1.9	38.3	21.5	7.10E+04	4.85	107.1	59.2
M1	S	71	1.3	47.2	20.2	6.39E+04	4.81	117.0	73.1

Ultimate Properties

Asphalt Binder Cracking Device (ABCD)

ABCD testing was performed on all samples for which test specimens could be successfully molded. Data from ABCD testing is shown below in Table 4, with blue-shaded rows showing results for polymer-modified samples. For the modified Material B1, box samples and a southern exposure sample were evaluated, whereas for Materials J1 and M1 only box samples were tested.

Table 4: Test Results for ABCD

Sample ID	Crack Temperature (T_{cr}), °C	Strain Jump, $\mu\epsilon$	Fracture Stress (σ_{AC}), MPa
B1-B (1)	-48.0	44.1	6.9
B1-B (4)	-50.8	92.8	14.6
B1-S (6), 1 st Replicate	-42.2	52.1	8.2
B1-S (6), 2 nd Replicate	-41.8	65.1	10.2
J1-B (40)	-20.4	20.3	3.2
J1-B (41)	-22.2	20.0	3.1
M1-B (53)	-25.2	14.8	2.3

The results in Table 4 offer three key takeaways:

- 1) The polymer modified material showed significantly lower cracking temperatures than the unmodified (oxidized) binders. This follows the general trend observed from the rheological testing of polymer-modified binders – that they showed greater relaxation properties (i.e., higher phase angles) at high stiffness levels.
- 2) Fracture stress – an indicator of fracture strength – was greater for the polymer modified material than for the unmodified (oxidized) binders. Strain jump, which is used to calculate fracture stress, was also higher, indicating that the polymer modified binders were able to sustain greater thermal strain (i.e. higher thermal strain tolerance) prior to cracking.
- 3) The aged polymer-modified binder (B1-S) showed an increase in cracking temperature of approximately 7 to 9°C and decrease in strain jump and fracture stress, as would be expected from an aged shingle compared to its unaged counterpart (B1-B). Although it was higher (warmer), it is significant to note that the cracking temperature was still substantially colder for B1-S than for either unaged, unmodified sample (J1-B and M1-B), illustrating the potential long-term benefits of polymer modification.

Correlating cracking temperature with rheological properties from a master-curve is challenging because of the temperature limits on the curve (usually -40°C), as well as the difficulty of obtaining reliable rheological data at extremely cold temperatures. However, comparisons of ABCD parameters to rheological relaxation and hardness parameters provide some useful trends, shown in Figure 33 and Figure 34.

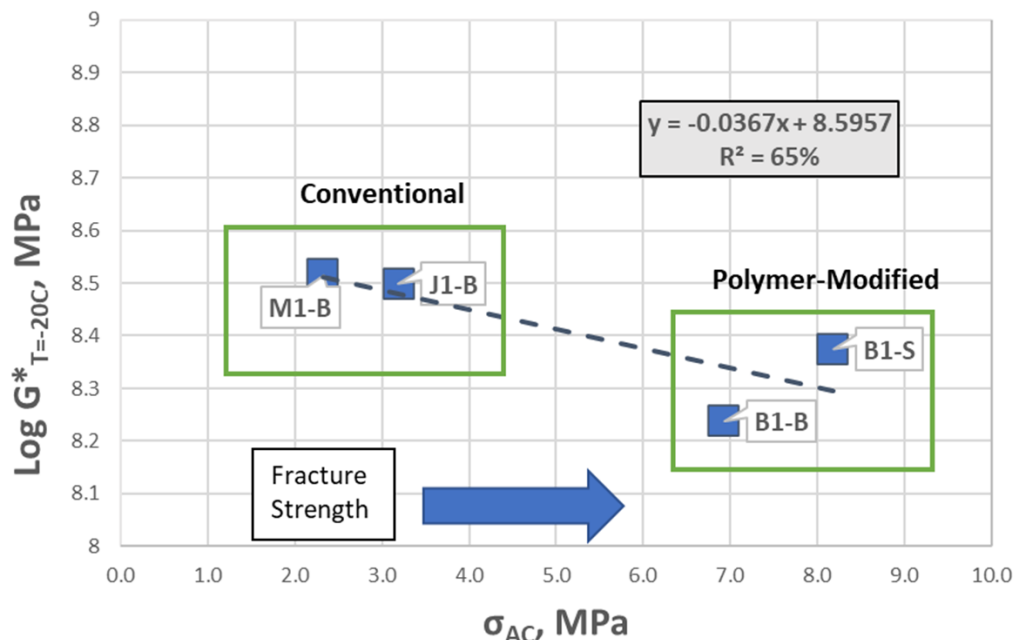


Figure 33: Log Stiffness (G^*) at -20°C (10 rad/s) vs. Fracture Stress

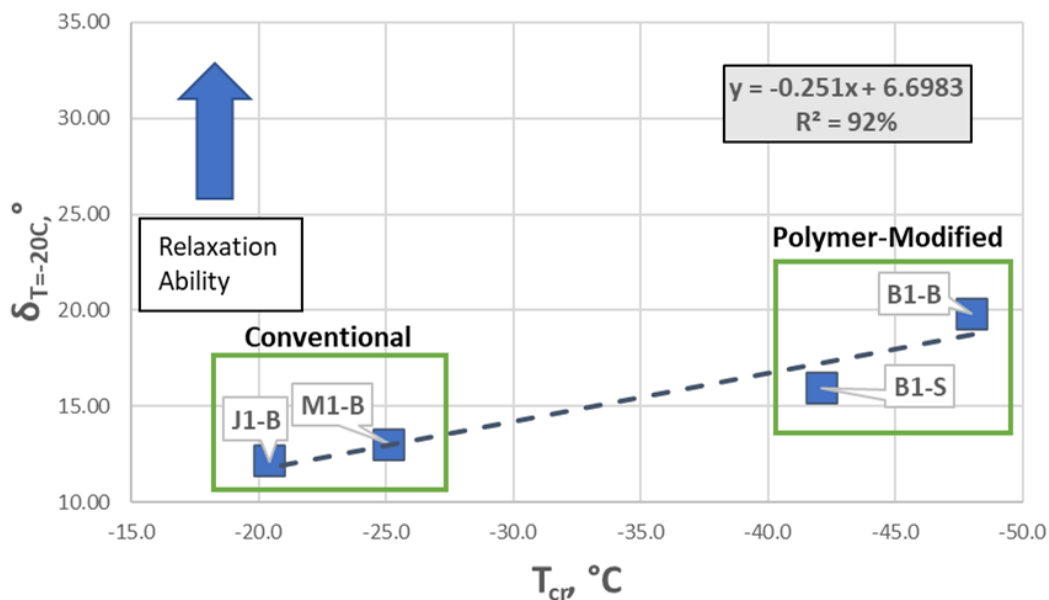


Figure 34: Phase Angle at -20°C (10 rad/s) vs. Cracking Temperature

The limited sample data set in this study shows a good correlation between phase angle at high stiffness levels and cracking temperature, indicating a relationship between relaxation and cracking susceptibility. More testing on other materials will be useful in illustrating these (and other) relationships.

Simplified Double-Edge-Notched Tension (SDENT) Test

The inclusion of the SDENT test in this research was intended to serve to characterize the fracture properties of a roofing asphalt binder. Two primary parameters are considered from the test: Total work of failure (W_t) and Fatigue/Fracture Performance Ratio (FFPR). The Total Work of Fracture, W_t , is derived by

plotting load as a function of displacement and then calculating the area under the curve. This value represents the tensile energy required to fracture the specimen. The FFPR is defined as the ratio of specific failure strain capacity (FSC) of a binder to a typical FSC value for a binder with a given modulus (Christensen and Tran, 2022). Thus, it is calculated as:

$$FFPR = \frac{FSC}{FSC^*}$$

where:

FSC = measured failure strain capacity of a specific binder

FSC* = failure strain capacity of a typical paving grade asphalt binder ($3.21 \times 10^6 |G^*|^{-0.788}$)

The calculation for FSC* illustrates that increasing stiffness (G^*) results in decreasing failure strain capacity. However, stiffness alone is not a sufficient indicator of fracture resistance, as two binders with similar stiffness values can show different strain capacities. The benefit of using the FFPR parameter is that fracture susceptibility is normalized with respect to stiffness; therefore, the inherent strain tolerance of binders can be compared independent of stiffness.

Previous researchers (Christensen and Tran, 2022) have used the SDENT test to calculate FFPR as the ratio between specimen extension (E) and the binder stiffness (S) as a function of extension. In that instance, the equation for FFPR is then modified to:

$$FFPR = \frac{E}{AS^B}$$

where:

E = SDENT extension to a given failure criteria

A, B = power law coefficients defining relationship between extension and stiffness

S = initial stiffness

Research reported in NCHRP Report 982 (Christensen and Tran, 2022) empirically determined coefficients A and B to be 48.0 and -0.371, respectively, while initial stiffness was defined as S after 3 seconds of loading. Additionally, extension was defined as displacement to 20% of the maximum load (post-peak). This model was used for calculating FFPR in this study, with the exception being that extension was defined as displacement to failure (i.e., specimen rupture) due to clear specimen ruptures after displacement.

One polymer-modified binder (G1) and one oxidized binder (M1) were chosen for evaluation using the SDENT test. Unfortunately, testing on M1 showed that the brittleness of the material would not allow for the generation of meaningful data due to the very small extension to failure. Data for G1 is shown in Table 5 and Figures 35-37. It can be seen from these figures, when multiple temperatures are used, that the maximum load is largest for the cold temperatures and the displacement is largest for the warmer temperatures.

Total extension to failure was used to calculate FFPR so that this value could be compared to total work of failure (i.e., area under the load vs. displacement curve). The correlation is strong between these two values (Figure 38) and is consistent with rheological data for G1. The southern exposure for Sample G1 showed greater aging and thus more susceptibility to failure through lower required energy for fracture.

Table 5: SDENT Test Data for Material G1

Material	Temperature, °C	Specimen	W _t , (kJ)	W _t , (kJ), Ave.	FFPR ¹	FFPR, Ave. ¹
G1-B	10	10C-1	9.79E-04	9.79E-04	1.98	1.98
		15C-1 15C-2	1.59E-03 1.51E-03		1.55E-03	
	20	20C-1	1.52E-03	1.68E-03	2.73	3.00
		20C-2	1.82E-03		3.21	
		20C-3	1.71E-03		3.06	
	G1-N	20	20C-1	1.27E-03	1.22E-03	2.07
20C-2			1.22E-03	2.19		
20C-3			1.16E-03	1.80		
G1-S	10	10C-1	9.37E-04	8.87E-04	0.62	0.60
		10C-2	8.37E-04		0.57	
	15	15C-1	1.14E-03	1.09E-03	1.13	1.09
		15C-2	1.04E-03		1.05	
	20	20C-1	8.98E-04	9.34E-04	1.12	1.20
		20C-2	9.70E-04		1.28	
	25	25C-1	6.97E-04	8.23E-04	1.16	1.34
		25C-2	8.72E-04		1.47	
25C-3		9.00E-04	1.40			

¹Calculated from total extension to failure

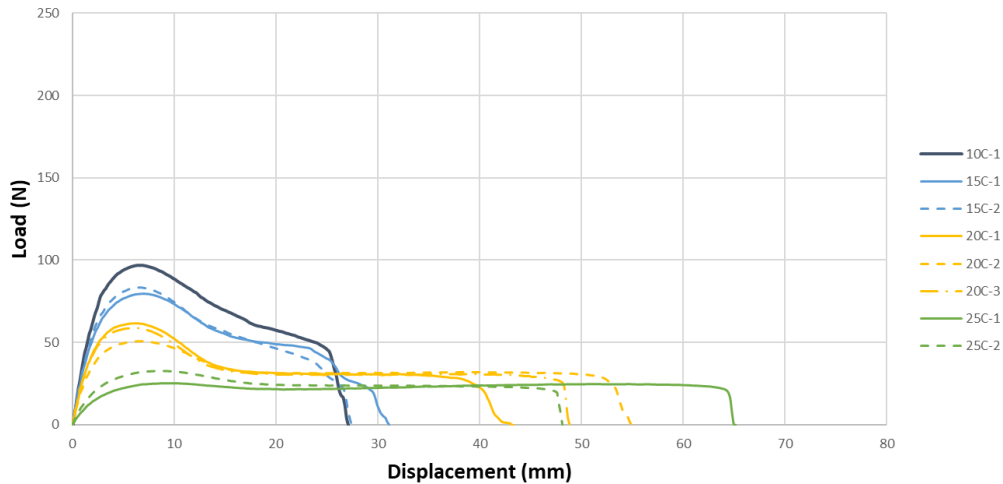


Figure 35: SDENT Test Results – Load vs. Displacement Curves for G1-B

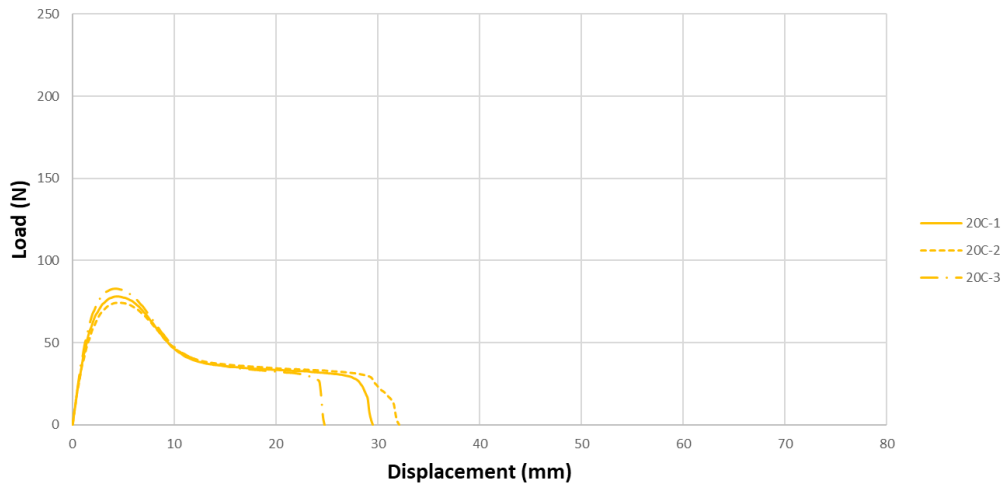


Figure 36: SDENT Test Results – Load vs. Displacement Curves for G1-N

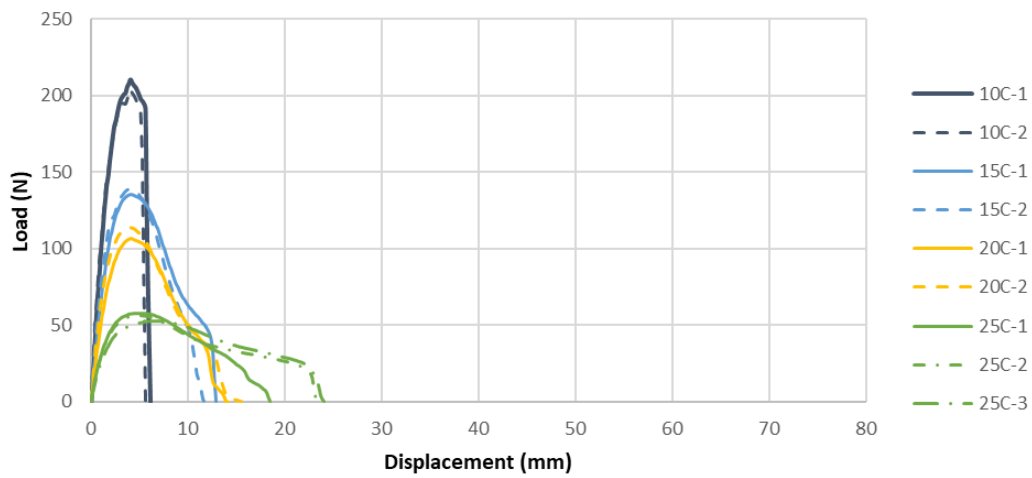


Figure 37: SDENT Test Results – Load vs. Displacement Curves for G1-S

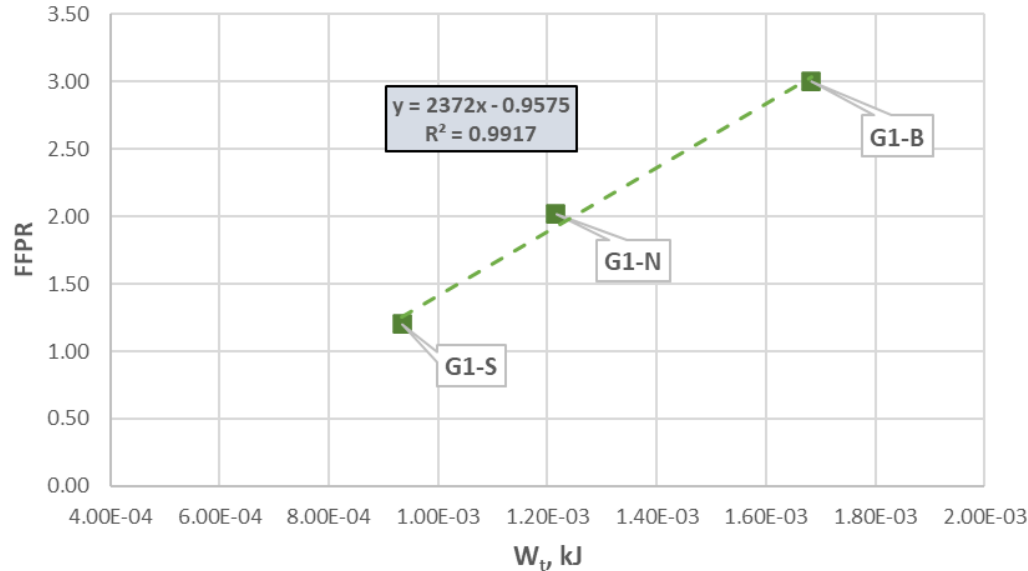


Figure 38: FFPR vs. W_t for Material G1 at 20°C

Modified Binder Yield Energy Test (modified BYET)

As previously noted, the BYET procedure was modified to better evaluate the materials of this study. One additional goal of the modified BYET procedure was to generate FFPR values for the other materials that could not be tested using the SDENT procedure due to high brittleness, limited temperature control, and/or limited amount of material. Through trial and error, a methodology for testing and analysis was developed that produced viable FFPR values for the available aged materials. The testing was performed following the procedure in Appendix A at using a rotational speed of 0.05 RPM and a temperature where the relaxation modulus was equal to 10 MPa, defined as $T_{G(t)_{int}=10MPa}$. The strain to peak stress (τ_{Peak}) was recorded, which was determined to be the binder “yield point” (point of failure). Strain was defined as the rotation of the specimen with respect to the circumference of the 8-mm test plates (γ_R). This was used instead of shear strain because it correlated better with SDENT. The “Binder Yield Energy” (BYE) was calculated by fitting a fourth-order polynomial curve to the stress-strain curve and finding the area under the curve up to τ_{Peak} . The relaxation modulus function, $G(t)$, was plotted using a power curve trendline fitted to the log stiffness/time function in the form of $\log y = a (\log x)^b$. FFPR was calculated in a similar manner to that used for the SDENT tests, using the equation below:

$$FFPR = \frac{E}{A7^B}$$

where:

- E = Rotational extension to peak stress, mm
- A, B = power law coefficients defining relationship between extension and stiffness
- 7 = log of targeted initial stiffness (10 MPa)

The stiffness at the binder yield point – $\log G(t)$ at $t=\tau_{Peak}$, defined as $G(t_{Peak\tau})$ – was determined from the corresponding power law fit calculated earlier. The resulting data is shown in Table 6.

Table 6: Data from Modified BYET

Sample	E, mm	Log G(t)int., Pa	Test Temperature, °C	BYE, MPa	FFPR	Log G(t _{peak}), Pa
B1-B	12.50	6.68	8.1	242.0	1.99	5.00
B1-S	5.86	6.82	18.1	114.0	0.84	5.34
G1-B	14.05	6.06	21.6	138.0	2.49	4.75
G1-N	12.57	6.63	27.8	122.6	1.98	4.66
G1-S	7.92	6.40	31.4	92.8	1.30	5.04
J1-B	0.59	6.93	34.3	6.8	0.08	6.12
J1-S	0.31	7.01	45.9	3.2	0.04	6.36
M1-B	2.03	7.02	32.5	30.3	0.28	5.97
M1-N (1)	1.17	6.94	38.3	18.1	0.16	5.93
M1-N (2)	0.96	6.98	38.3	17.6	0.14	6.04

Figure 39 and Figure 40 show the stress-strain and G(t) curves from the modified BYET procedure. Figures 41-43 show that FFPR has strong relationships with BYE, log G(t_{peak}) and $\delta_{G^*=10 \text{ MPa}}$.

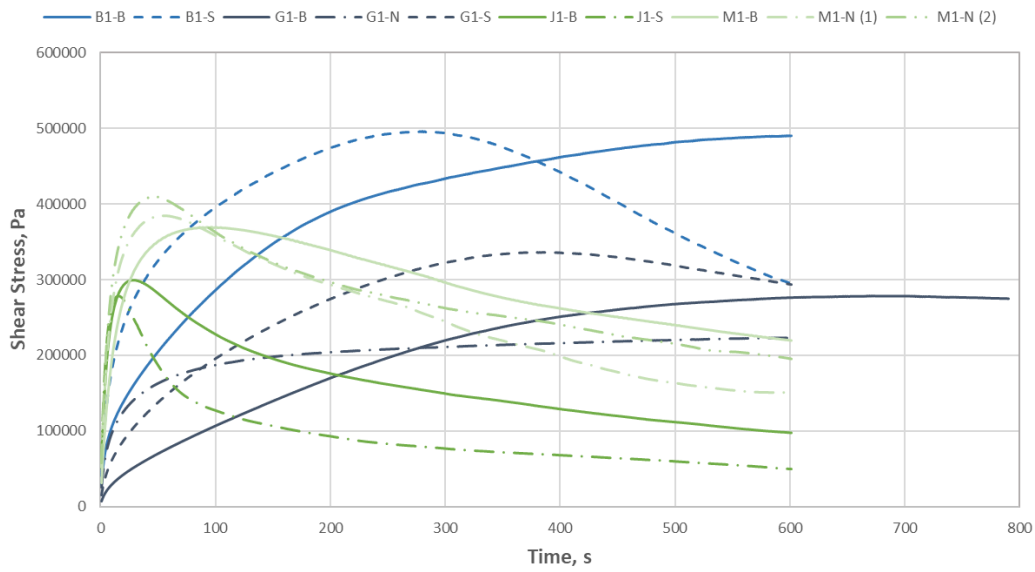


Figure 39: Stress-Strain Curves from Modified BYET

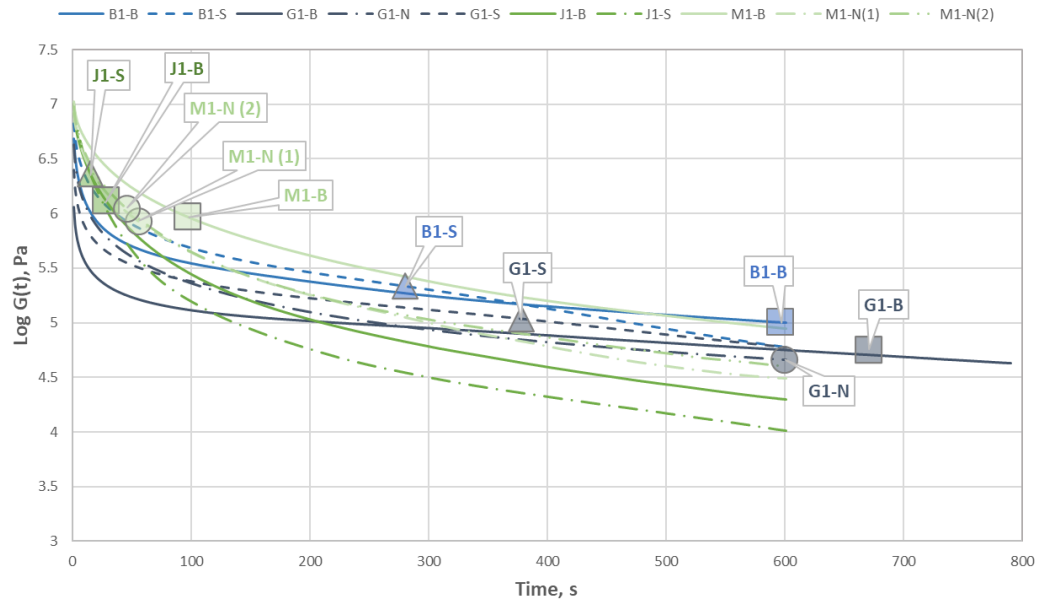


Figure 40: Log G(t) Curves from Modified BYET

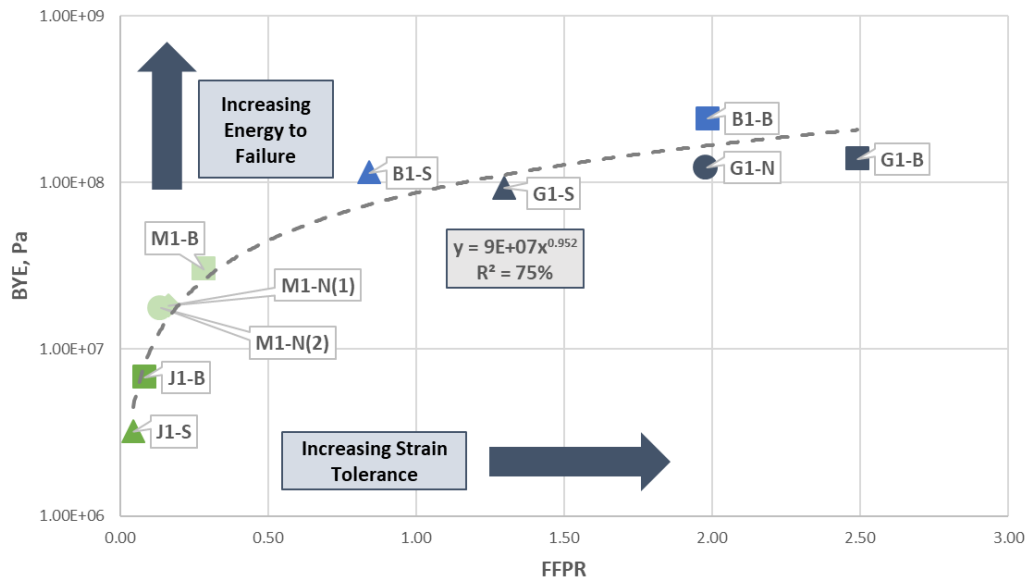


Figure 41: Relationship between FFPR and BYE

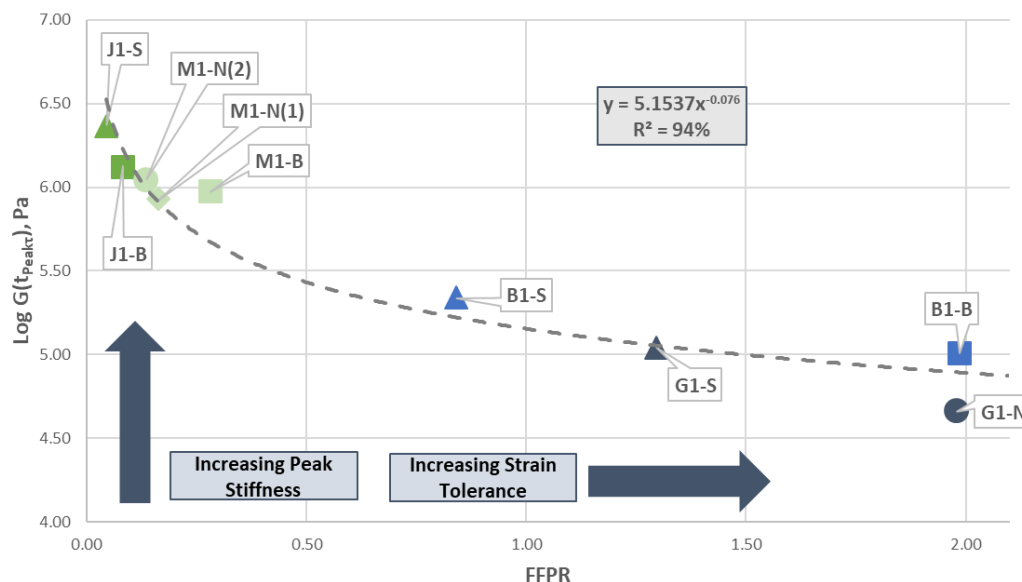


Figure 42: Relationship between FFPR and $\text{Log } G(t_{\text{peak}})$

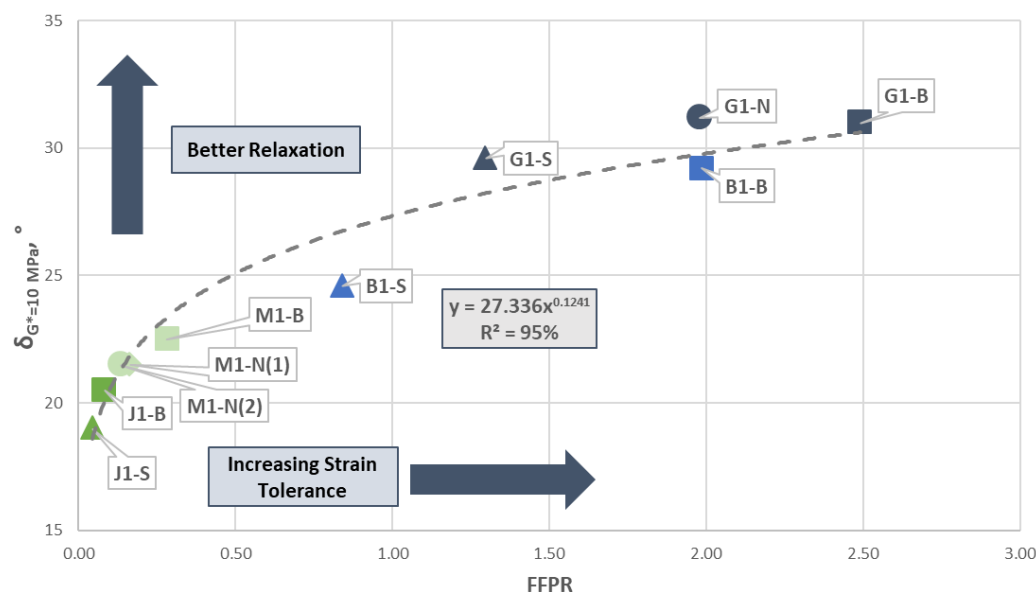


Figure 43: Relationship between FFPR and $\delta_{G^*=10\text{MPa}}$

Poker Chip Test

The Poker Chip test was evaluated by conducting tests at 0, 10, 20 and 30°C. In the initial experimentation it was noticed that the data produced did not have a clear definition of the start time, (see Figure 44). In addition, in a test that uses a constant load application, the shape of the stress-strain curve should have a reducing tangent modulus. In the initial tests, the tangent modulus slowly increased at the start of the test. This response happens due to slack in the equipment, necessitating the development of a modification to the data analysis to reduce the effect and more appropriately define the start time of the test. The modification used by the research team involved fitting a straight line from the displacement between 40 and 60% max load and then projecting a line back to the x-axis, thus obtaining a displacement that would

correspond to the point in the test where the load would start without any slack. This procedure could then be used to define a zero-load time and enable the definition of the period from the effective start of the load to the maximum load. The modification to the data analysis procedure is illustrated in Figure 45.

The binder relaxation modulus, $G(t)$, was determined using the two loading times (peak and post-peak 80%) from the rheological master-curves that were developed. The $G(t)$ was assessed from fitting relaxation spectra to the data set and then using this data to convert the complex modulus and phase angle (G^* and δ) to a relaxation modulus, $G(t)$. Sample G1-S (36) was tested first, and the results are presented in Figure 46. It can clearly be seen that the load level is higher and the displacement lower for the colder temperatures. As the sample test temperature is increased (reducing stiffness) the type of failure changes from brittle to ductile behavior. The “ductility” (displacement in this test) was determined at both the peak stress and at the post-peak condition where the strain had dropped to 80% of the peak value. At low temperature/ high stiffness, these values were coincident, whereas at higher temperatures these values diverged. Figure 47 shows the relationship between parameters derived from the Poker Chip test and temperature or binder stiffness, $G(t)$.

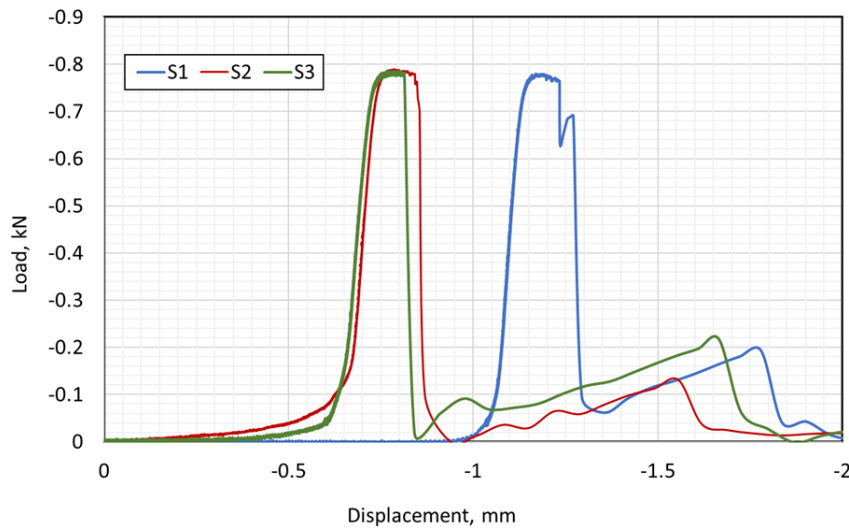


Figure 44: Initial Trials using Poker Chip Tests Showing Stress Starting at Different Displacements

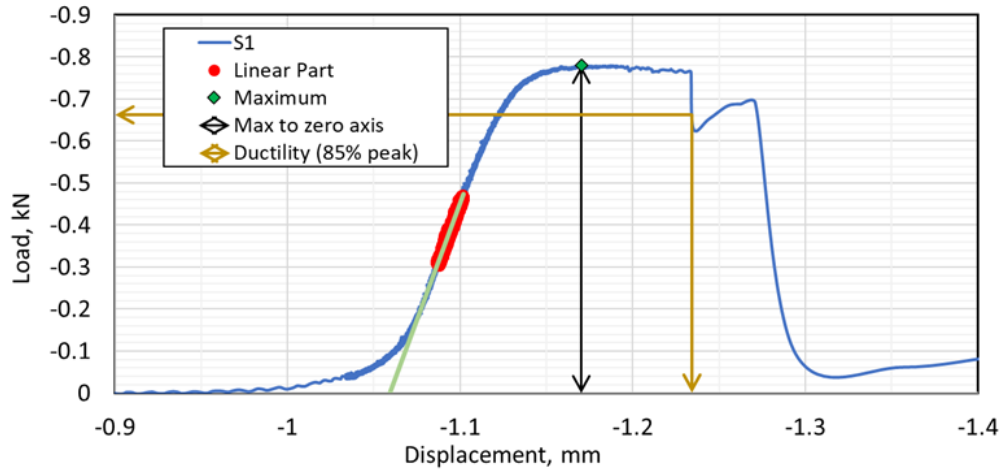


Figure 45: Load between 40 and 60% of Maximum used to Define the Start of the Test

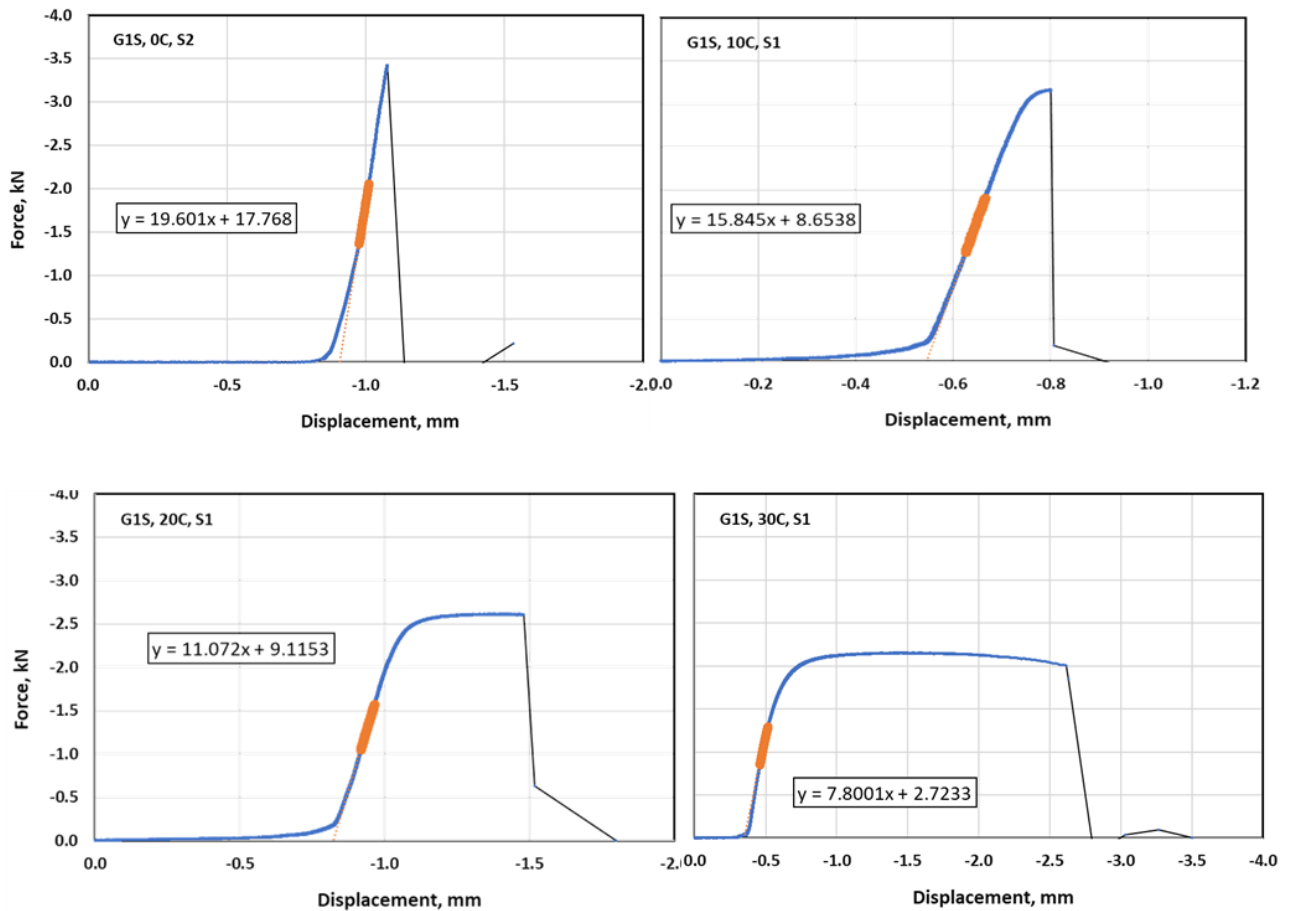


Figure 46: Poker Chip Test Results for Material G1-S (6) at 0, 10, 20 and 30°C

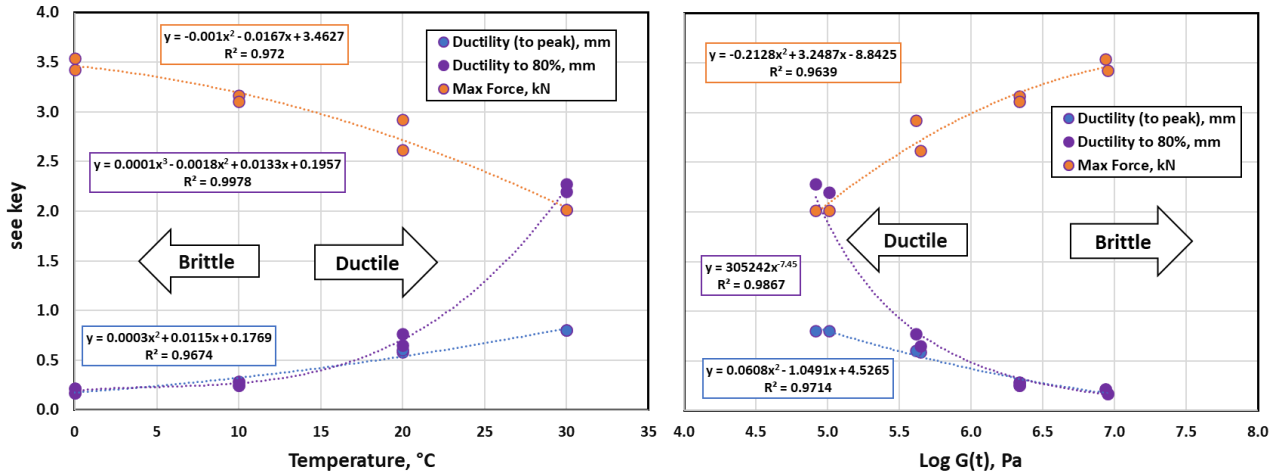


Figure 47: Poker Chip Test Results vs. Temperature and Binder Stiffness, G(t)

Based on the analysis of Material G1, the testing was extended to other materials in the sample set. However, acceptable results could not be obtained with the stiffer Material M1 due to apparent debonding (adhesive failure) and/or micro-cracking during the cooling process. This occurred at all temperatures, including the highest considered in the test regime (Figure 48). The data produced in this testing at the two extreme temperatures are shown in Figure 49.

It was realized that some significant test modifications would be required to further pursue the use of this procedure for the roofing asphalt binders in this study. Since the Poker Chip test could not be equally applied to materials of varying stiffness, this testing was discontinued after the evaluation of Material M1.



Figure 48: Poker Chip Test for Material M1-S (71) at 30°C, Showing Issues with Debonding during the Procedure

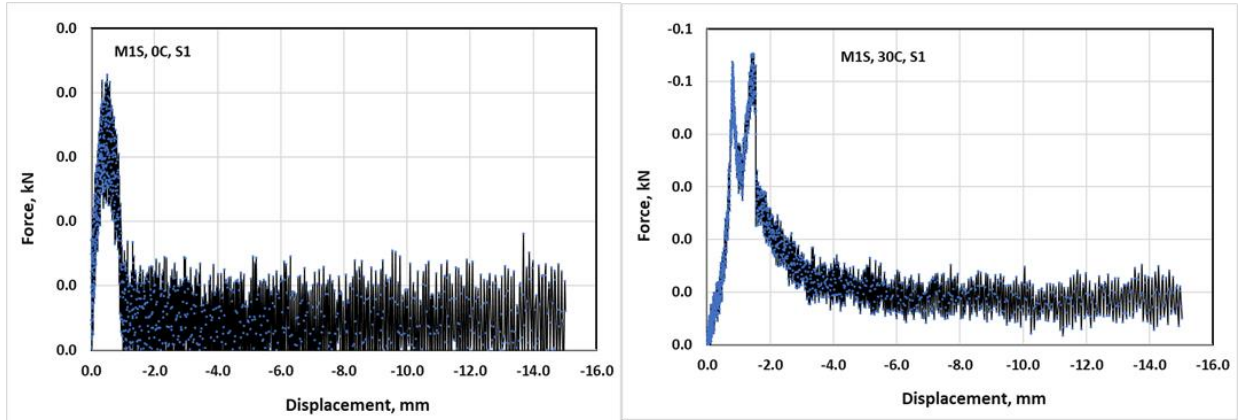


Figure 49: Poker Chip Test Results for Material M1-S (71) at 0 and 30°C

Discussion

ABCD

While some data was generated from the ABCD procedure, most samples could not be molded into viable test specimens, which limited the value of the ABCD test in the evaluation of materials in Phase I of the study. The inability to mold viable specimens was attributed to the use of stiffer binders than are normally evaluated using the test procedure. As the stiff roofing asphalt binders were poured into the standard silicone ring mold, they cooled very rapidly upon contact with the mold surface, creating non-uniform and often discontinuous rings of asphalt binder. This was especially true near the notch on the silicone mold that creates the cracking point in the asphalt binder ring, since the asphalt cannot flow underneath the notch to form the hole at which the crack is intended to form, as shown in Figure 50. The ABCD test is highly dependent upon uniformity in the asphalt binder ring, especially at this cracking point, to detect a jump in strain and determine a cracking temperature. Furthermore, non-uniform specimens will also result in higher variability between test specimens, which is not ideal.



Figure 50: Poorly Molded Aged Roofing Binder Specimen for ABCD Test

To mitigate this issue, the stiffer roofing asphalt binders would need molds that can be placed into an oven to allow the binder to flow around the ring mold and form a uniform specimen. While not something recommended in standard practice, a similar procedure is often used for molding extremely stiff BBR specimens (described in AASHTO T313). In this procedure, binder specimens that cool rapidly upon contact with the mold are placed into an oven after molding, allowing the binder to flow into the mold and form a uniform beam specimen. A similar practice could be followed with the ABCD molds, if not for the fact that the silicone mold and strain gauge are not rated for exposure to the elevated temperatures that would be encountered in an oven environment.

One potential alternative is the use of a steel ring mold, designed for use with stiffer materials, such as roofing asphalt. These molds use a slightly different procedure for generating specimens, primarily in the fact that they may be placed into an oven at elevated temperature to facilitate uniform specimen molding. While not known to be commercially available, prototype molds have been offered to the Asphalt Institute by industry research colleagues for use in a potential Phase 2 of this study.

Modified BYET and Rheological Properties

Following the procedures discussed in NCHRP Report 982, an asphalt binder with a FFPR value of 1.0 is considered to have average strain tolerance for a given stiffness, because the measured FSC is equal to the FSC of a typical binder of that stiffness (FSC*). Using this benchmark, we can see that the modified binders (B1 and G1) showed greater inherent strain tolerance than the conventional binders (J1 and M1), indicated in the data in Table 6.

The southern exposure of G1, Sample G1-S (36), showed greater loss of strain tolerance than the northern exposure, which is consistent with rheological data shown in Figure 51. Sample B1-S (6) had an FFPR value of 0.84, less than that of both G1 exposures. Again, this is consistent with data from rheological testing; at the 10 MPa stiffness level, Sample G1-S (36) was shown to have a higher phase angle than Sample B1-S (6), indicating the connection between relaxation and strain tolerance.

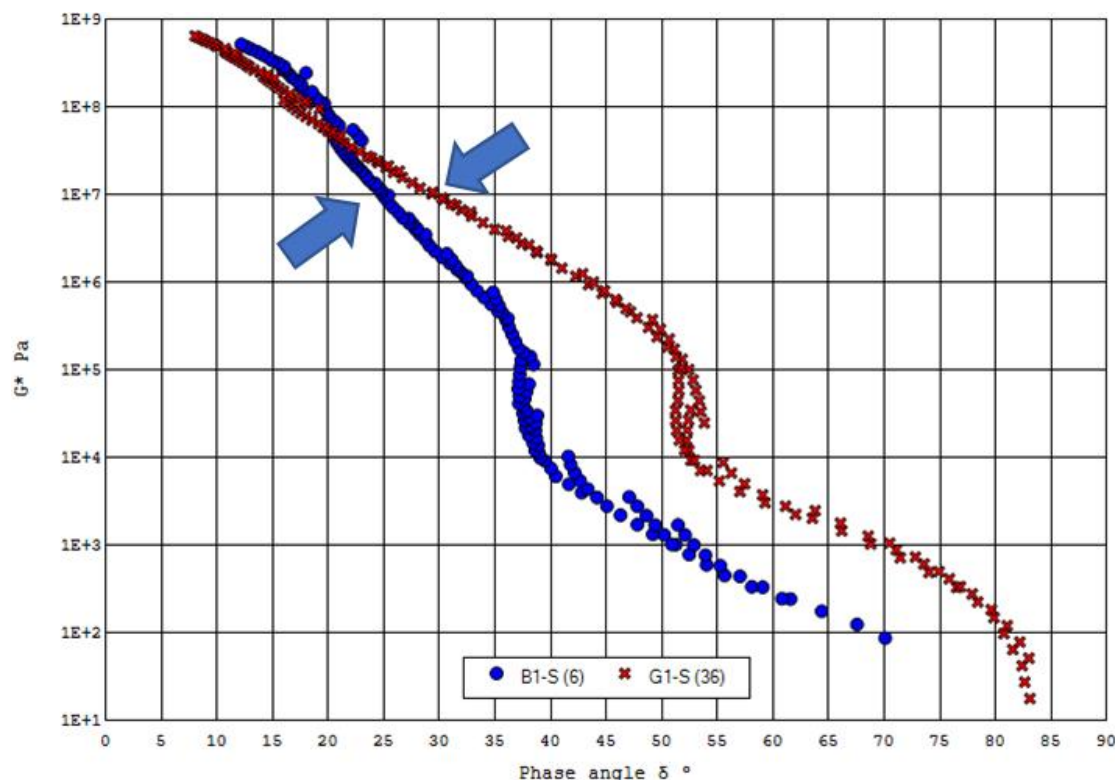


Figure 51: Black Space Plots of B1-S (6) and G1-S (36)

By testing the aged and unaged samples using the modified BYET procedure, a comparison of the change in strain tolerance over the course of the life cycle of a roofing asphalt can be made. If an FFPR of 1.0 is considered a benchmark for average strain tolerance, the following observations can be made:

- 1) While the aged, oxidized coatings showed lower-than-average FFPR values at the end of the aging cycle, they also began the aging cycle with relatively low FFPR values. Very little change in strain tolerance appears to occur during aging. This observation makes sense considering the high level of oxidation that occurs in the production of a roofing asphalt coating before it is put into service as a component of the shingle structure.

- 2) There appeared to be more reduction in strain tolerance during aging with the polymer-modified materials than with the oxidized materials. The box samples for Materials B1 and G1 showed very high FFPR values. While those values dropped considerably for the aged samples obtained from the roof racks, two of the three harvested polymer-modified shingles still indicated FFPR values greater than 1.00 at the end of the aging cycle.

This response described above demonstrates that a large portion of strain tolerance from polymer modification appears to be retained in an aged shingle, even though there is a larger magnitude in loss of strain tolerance from binder aging when compared to an oxidized material. Conversely, the oxidized samples showed a small loss in strain tolerance, but also had lower-than-average strain tolerance after initial installation. All aged polymer-modified materials showed higher strain tolerance at the end of the aging cycle than any unaged oxidized material.

Plotting the change in relaxation modulus, $G(t)$, as a function of shear strain or loading time, as shown in Figure 40, spatially demonstrates the fact that modified Materials B1 and G1 appear able to sustain shear stress at longer loading times than unmodified Materials J1 and M1, highlighting the benefit of polymer modification and an indication of ability to relax stress under loading. Steeper tangent line slopes to the $G(t)$ power curve fit at peak stress (seen in Figure 41) can be observed for the unmodified binders with shallower tangent line slopes to the $G(t)$ curve at peak stress observed for the modified binders. The implication is that the unmodified asphalt binders in this study reached a yield point during rapid change in shear stress after shorter loading times, while the modified binders were able to tolerate the large rise in shear stress at initial loading and did not reach a yield point until loading time significantly increased. The differences in these yield points (both in magnitude and manifestation) show the difference in strain tolerance between the two sample types (oxidized and modified).

From the strong relationship between FFPR and phase angle at 10 MPa of stiffness, it is observed that a FFPR value of 1.0 equates to a phase angle of approximately 27.3 degrees. Although this finding is based on a limited data set, it appears that it may be a useful tool in future work in establishing guidelines. It should be noted that a phase angle of 27 degrees approximates to an m -value (as measured in the BBR) of 0.300 (Rowe, 2014) and was a value initially suggested as a parameter correlated to cracking in road pavements by other researchers (Migliori et al., 1999).

FFPR and Approach Considered in SDENT and MBYET

The analysis procedure for FFPR was initially proposed by Christensen and Tran (2022) by considering the analysis approach originally offered by Heukelom (1966). Heukelom demonstrated that for all practical purposes the fracture strength (strain and stress at break) for most paving grade binders could be considered as a master-curve relating strain and stress to the binder stiffness, as shown in Figure 52.

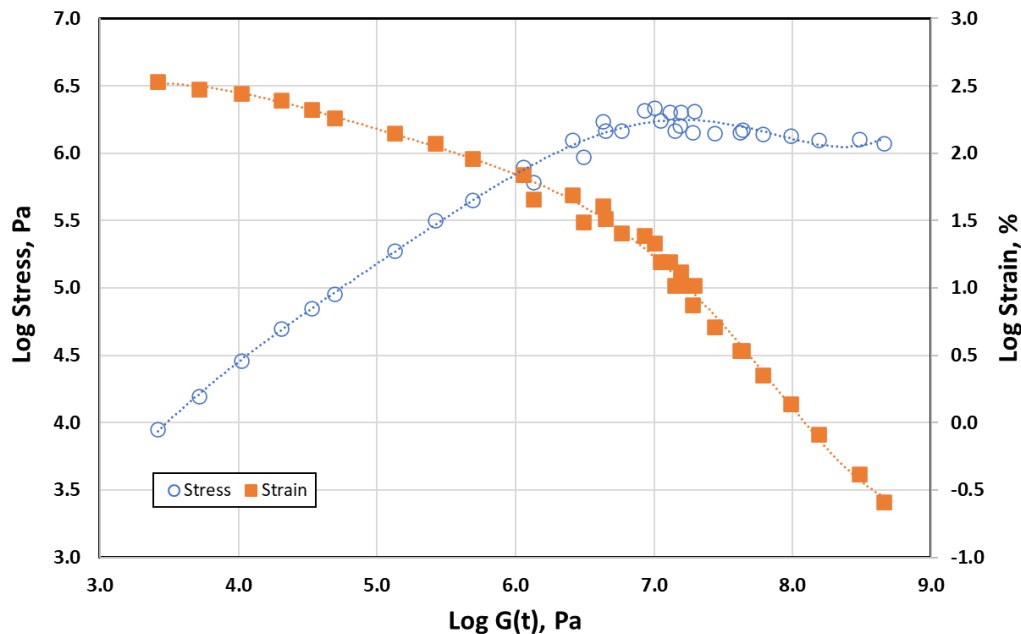


Figure 52: Stress and Strain at Break, after Heukelom (1966)

The FSC* relationships proposed by Christensen and Tran (2022) produced straight lines on the plot of log strain versus log G(t), which is reasonably consistent with Heukelom’s data in the region of log G(t) from 5.5 to 8. Thus, the FFPR calculated using the FSC* equation will be different than what is obtained when compared directly to that produced by Heukelom (Figure 53). The equation used in the modified BYET analysis has a similar relationship to that applied with the SDENT method. If test data from the modified BYET is compared to the data generated by Heukelom it can be observed that the modified binders all lie above the relationship, whereas the unmodified roofing binders are all below the curve (Figure 54). For comparison purposes, some data obtained from Direct Tension tests (Rowe and Sharrock, 2004) were added to Figure 54 (illustrated by “+” signs), indicating consistent behavior with the data produced by Heukelom (1966). Heukelom initially suggested that the data produced for log strain could be modelled by two straight lines whereas Christensen and Tran (2022) have adopted a single straight line. In this research, a high order polynomial fit was used as it was considered more descriptive of the data. It is possible that other relationships such as Gompertz (1825), Richards (1959) and/or other sigmoid type relationships could also be used to fit the data. It should be noted that if data is compared to these different relationships, numerical differences will exist in the value calculated for the FFPR.

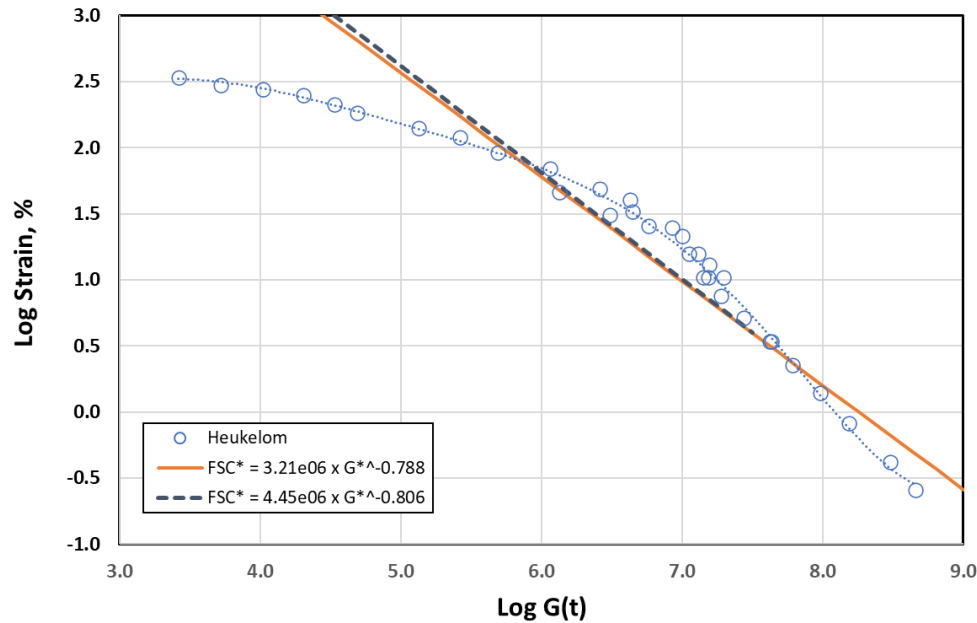


Figure 53: Heukelom versus FSC*, Defined as Failure Strain Capacity of Typical Asphalt Binder (SDENT, $3.21 \times 10^6 |G^*|^{-0.788}$) and (BYET, $4.45 \times 10^6 |G^*|^{-0.806}$)

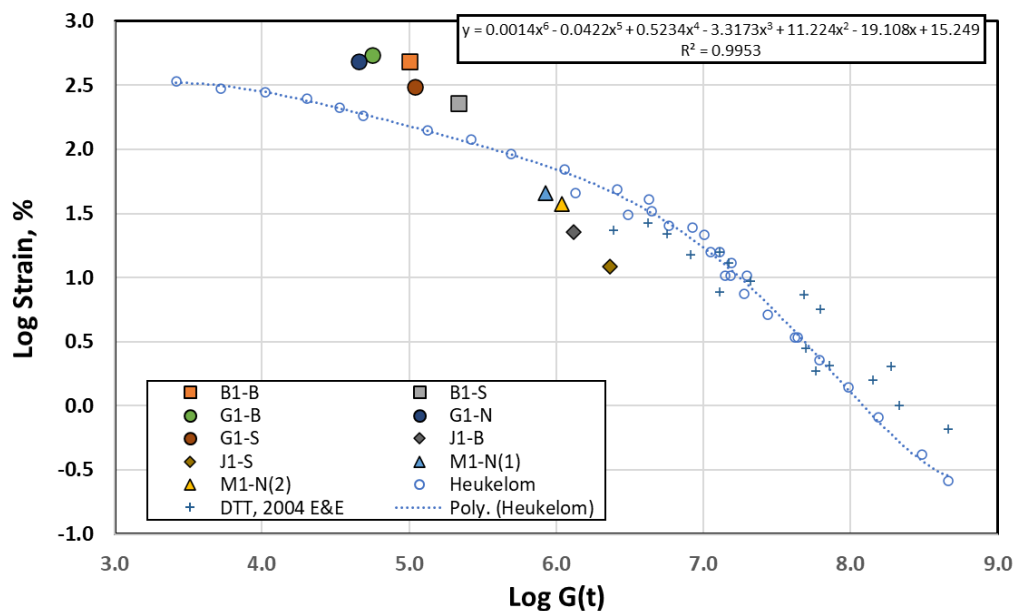


Figure 54: Data from BYET compared to the Heukelom curve

The ratio of performance compared to the Heukelom-type curve is what was initially considered by Christensen and Tran (2022) in their NCHRP research project. In the analysis of the modified BYET test, it is believed that the review of the criteria based upon the original approach represents a more fundamental analysis. This aspect will be further considered in an extension of this work as additional materials are tested and additional data is obtained to develop FFPR results. FFPR in this report has been expressed using linear values but conceptually it could be considered as the log of the strains at the particular stiffness levels, consistent with the log-log style plot presented. The high level of correlation between the two methods used for FFPR (Figure 55) means that there should be no significant changes in the FFPR obtained

by the different methods. However, the research team believes that using the direct comparison to the Heukelom curve more accurately distinguishes the performance between the modified and conventional (unmodified) products.

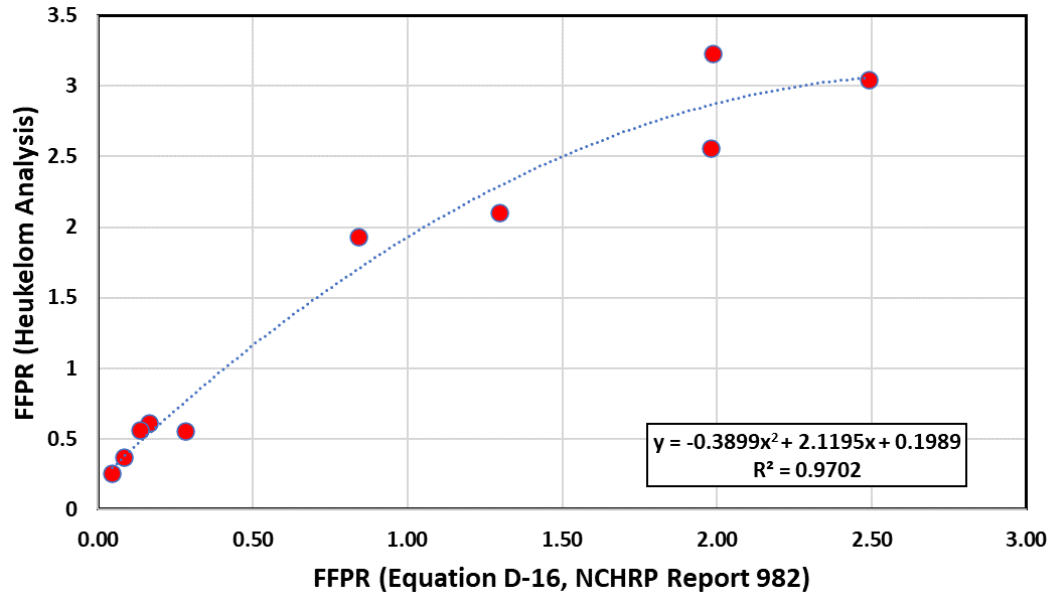


Figure 55: Alternate Methods of FFPR Calculation

Performance Review

Performance data was collected for the various study materials in 2008 after approximately 5.5 years in service. The data, shown in Table 1, included the total impact points and the percentage of those points with noted damage after testing. The ability of a hail stone to make an impression on a surface is hypothesized to be related to the stiffness of material. In this case a lower stiffness binder is more likely to be indented in some manner. The damage at an indent location and the ability to resist loss of granules (aggregate) and cracking is considered to be related to the ability of a binder to relax stresses caused by an impact. Thus, the research considered parameters that relate to this behavior in the higher stiffness region.

As discussed previously, the research team believed that the best rheological measure from the DSR to capture the relaxation properties was the phase angle at a stiffness of 10 MPa. The plot of this value versus the impact locations with damage is shown in Figure 56. These data appear to validate the hypothesis that the damage observed is related to stiffness and relaxation of the binder used in the shingle.

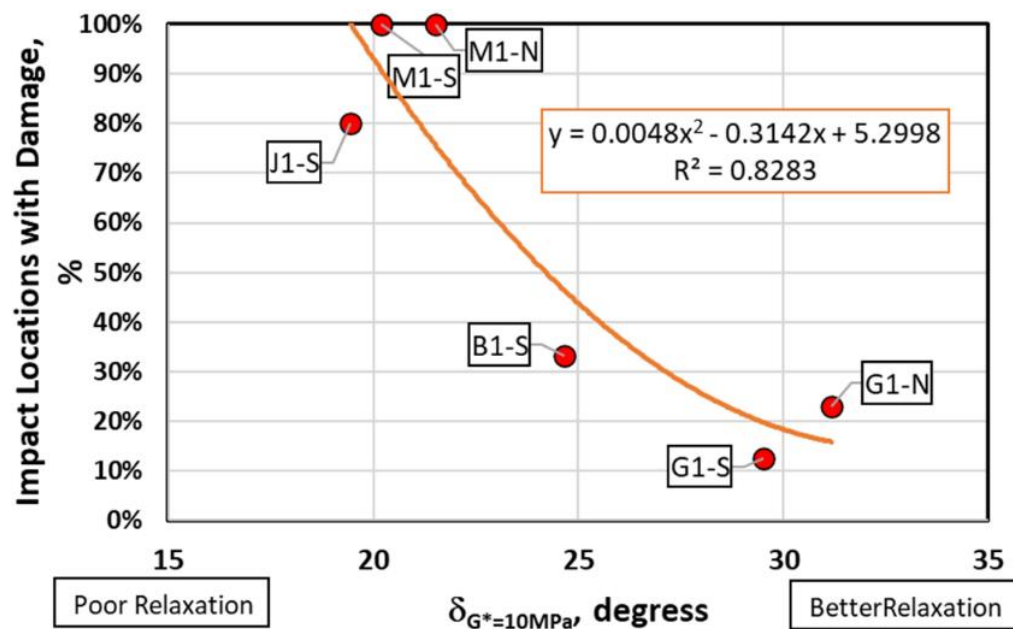


Figure 56: Impact Locations with Damage Following Testing after 5 Years of Exposure on Aging Decks

This hypothesis is further validated through the SDENT and modified BYET data, which also correlate well when considered at the intermediate stiffness value. Similar plots were developed in Figure 57 and Figure 58, showing the FFPR (a measure of strain tolerance) from the modified BYET versus the damage locations. For the sake of comparison, the relationship with both methods of calculating FFPR were applied (method based on NCHRP analysis method and a direct comparison to the Heukelom data set).

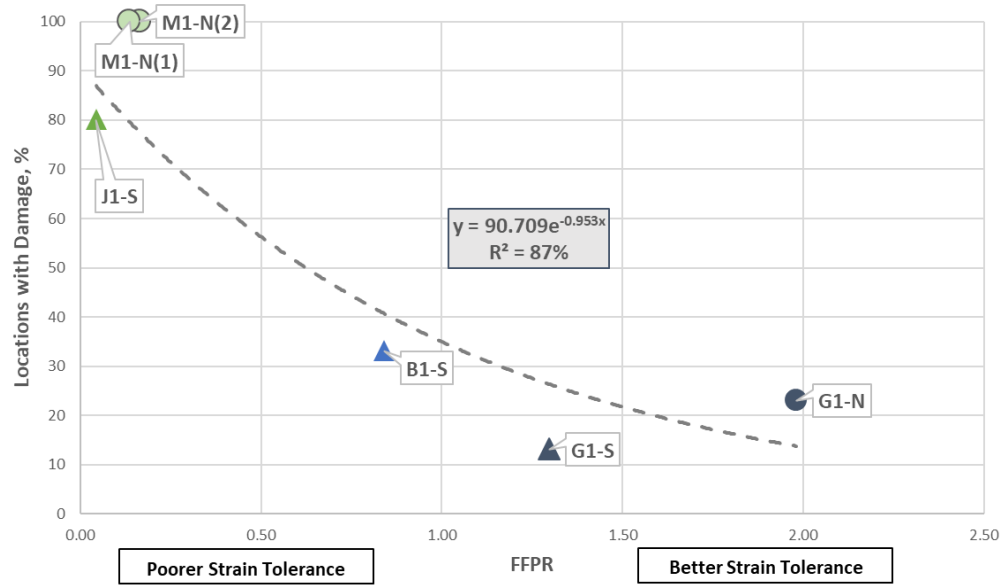


Figure 57: Impact Locations with Damage versus FFPR (NCHRP method)

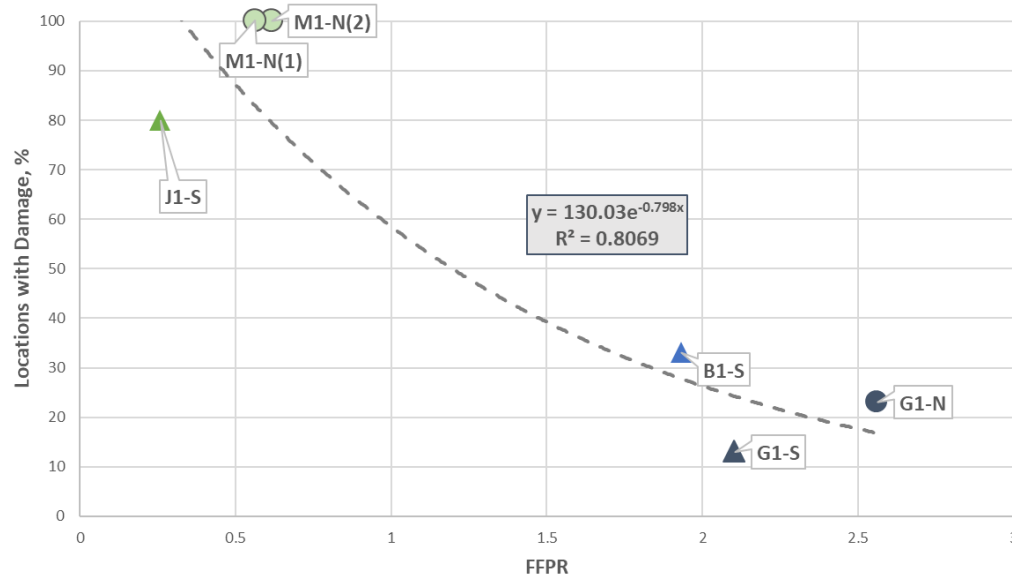


Figure 58: Impact Locations with Damage versus FFPR (Heukelom method)

Summary

Rheology

Complex modulus and phase angle data were obtained and analyzed for the samples in this study. In addition, BBR data sets on some materials were also obtained and analyzed. From the rheological testing the following comments can be made:

1. BBR testing with stiff roofing products is difficult to perform and little additional benefit was obtained from the inclusion of BBR data in the analysis.
2. The use of 4-mm parallel plate rheology using the DSR showed little value for the materials tested compared with the more commonly used 8-mm parallel plate rheology. Consequently, this method was not pursued after some initial experimental work. In addition, it should be noted that 4-mm rheology will be more difficult to implement in laboratories since great care is needed in preparing specimens and performing the test.
3. The development of master-curves was successful for all the roofing materials. In the analysis of model parameters, and other fitting parameters, the following was concluded:
 - a. The use of the Christensen-Anderson model for roofing grade binders was generally unsuccessful.
 - b. The determination of a cross-over modulus (G_c) typically occurred at a stiffness that was too low to be associated with cracking. For some modified materials this proved to be a very unreliable indicator of performance.
 - c. Better indicators of the shape of the master-curve in the high stiffness region were considered to be the phase angle (δ) at a constant modulus (10 MPa) and/or the properties associated with a phase angle (δ) of 27 degrees. The temperature at which the phase angle is 27 degrees can also be evaluated with ease and this was well correlated with observed impact damage.

Ultimate tests

Four ultimate tests were considered:

- 1) Asphalt Binder Cracking Device (ABCD),
- 2) Simplified Double-Edge Notched Tension Test (SDENT),
- 3) Binder Yield Energy Test (BYET), and
- 4) Poker Chip Test.

Based on the evaluation of these tests, the following comments can be made:

1. ABCD
 - a. Specimen preparation using the silicone molds was difficult and, in some cases, it was clear that binder had not flowed into the mold properly, resulting in poor specimens.
 - b. The within-laboratory repeatability was higher than expected.
 - c. The data appeared to rank the materials tested in the correct manner.
 - d. Alternate metallic molds possibly could be used to provide viable specimens and repeatable data sets.
2. SDENT

- a. An acceptable result was produced with a softer sample, but the stiffer sample (M1) could not be evaluated due to brittle behavior. Consequently, it seems unlikely that this method, in its current form, should be pursued for additional testing with roofing-asphalt products.
3. **BYE Test**
 - a. This test required some modification to enable tests to be performed. The modifications and draft method are given in an appendix to this work.
 - b. The testing temperatures selected resulted in stiffness at the failure condition which were significantly lower than initially targeted value (10 MPa).
 - c. The energy calculations showed significant correlation with rheology and hail damage.
 - d. FFPR showed a good relationship with rheology and hail damage.
 - e. Ongoing research may improve the procedure to enable testing in the appropriate stiffness region.
 4. **Poker Chip Test**
 - a. This test enabled the evaluation of ductility versus temperature and binder stiffness for a lower-stiffness roofing binder.
 - b. A high stiffness, oxidized binder was not able to be evaluated due to debonding (adhesive failure) that occurred during the specimen preparation.

A key objective of this research was to advance the science around the durability of asphalt shingles, specifically the properties of the coating asphalt used in residential roofing. Phase 1 of the research, the subject of this report, was designed to evaluate the aging of the roofing asphalt binder and the change in its physical properties as a result of aging which may lead to brittleness, cracking, and loss of granule adhesion. Phase 1 was intended to focus on identifying one or more parameters, preferably determined using standard asphalt materials testing equipment, that are hypothesized to relate to the durability of asphalt shingles.

The findings from Phase 1 of this research project indicate that rheology and failure tests can be used to characterize the effects of aging and the change in physical properties of roofing asphalt binders that may be related to shingle performance and durability – specifically damage (cracking) and loss of granule adhesion resulting from the impacts of hail. The two tests best correlated with performance in each category appear to be: (1) the phase angle (δ) at a constant modulus (10 MPa); and (2) the Fatigue/Fracture Performance Ratio (FFPR) and yield energy determined from the modified BYET procedure. Both procedures can be conducted using the DSR with conventional 8-mm parallel plate geometry.

Recommendations for Additional Study

Phase 1 of this research project was intentionally limited in scope to focus on evaluating various rheological and failure (ultimate) tests to determine roofing asphalt binder properties that could be related to aging and durability. Although Phase 1 was successful, the limited scope means that additional work is needed to fully validate the findings and to ultimately assist suppliers and purchasers of asphalt shingles in understanding what parameters they need to consider to provide enhanced durability and a longer life cycle for asphalt shingles.

The following are recommendations to consider as an extension to Phase 1 of the research.

Extension to Additional Roofing Materials

- 1) Additional materials made with other binders should be harvested and tested to extend the data set from the currently limited data.
- 2) Data from other studies should be combined with this work to further assess correlations that exist between rheological properties and performance.

Test Method Improvements

- 1) ABCD testing should be further evaluated using metal molds for the roofing asphalt samples.
- 2) Additional refinement to the BYET procedure and analysis methodology should be evaluated to fully assess the efficacy of the test method.

Climatic Assessment

- 1) The application of criteria to different climates needs consideration.

Acknowledgments

The authors gratefully acknowledge the financial support and project management offered by State Farm Mutual Automobile Insurance Company and the Asphalt Institute Foundation in the successful execution of this research. Thanks specifically to Doug Dewey and his colleagues with State Farm at The Research and Innovation Laboratory (TRAIL) for their assistance in identifying and collecting aged and unaged shingles, as well as offering insights on the test plan and results.

Disclaimer

The research described in this report was conducted for the Asphalt Institute Foundation under grant funding provided by State Farm Mutual Automobile Insurance Company. The analyses and technical opinions offered are those of the authors and do not necessarily reflect those of the Asphalt Institute Foundation, State Farm Mutual Automobile Insurance Company, Asphalt Institute, or the individual member companies of the Asphalt Institute.

References

Anderson, D.A, Le Hir., Y.M., Marasteanu, M.O., Planche, J-P., Martin, D. and Gauthier, G., “Evaluation of Fatigue Criteria for Asphalt Binders,” Research Record, 1766(1), 48-56. <https://doi.org/10.3141/1766-07>, 2001.

Anderson, R.M., King, G.N., Hanson, D.I. and Blankenship, P.B., “Evaluation of the Relationship between Asphalt Binder Properties and Non-Load Related Cracking,” Proceedings, Association of Asphalt Paving Technologists, 2011.

ARMA, “A Simple Guide to Understanding Your Shingle Roofing System,” Asphalt Roofing Manufacturers Association, <https://www.asphaltroofing.org/a-simple-guide-to-understanding-your-asphalt-shingle-roofing-system/>. Accessed 2023/06/11.

Bennert, T., Garg, N., Ericson, C., and Cytowicz, N., “Evaluation of Test Methods to Identify Asphalt Binders Prone to Surface-initiated Cracking,” Transportation Research Record, 2677(3), 897-910. 2022. <https://doi.org/10.1177/03611981221119191>

Christensen, D.W. and Tran, N., “Relationships Between the Fatigue Properties of Asphalt Binders and the Fatigue Performance of Asphalt Mixtures,” NCHRP Report 982, Washington, D.C.: Transportation Research Board, 2022.

EPA, “Sustainable Materials Management Basics,” United States Environmental Protection Agency, Website - <https://www.epa.gov/smm/sustainable-materials-management-basics>. Accessed 2023/06/11, Updated 2/6/2023.

Filonzi, A., Mohanraj, K., Trevino, M., Hazlett, D. and Bhasin, A., “Implementation of Improved Performance Grade (PG) of Asphalt Binders,” Technical Report 5-6925-01-1, The University of Texas at Austin, Center for Transportation Research, 2022.

Gompertz, B. “On the Nature of the Function Expressive of the Law of Human Mortality, and on a New Mode of Determining the Value of Life Contingencies,” Philosophical Transactions of the Royal Society. 115: 513–585. doi:10.1098/rstl.1825.0026. JSTOR 107756. S2CID 145157003. 1825.

Kriz, P., Campbell, C.M., Kucharek, A.S. and Varamini, “A Simple Binder Specification Tweak to Promote Best Performers,” Proceedings of the Sixty-Fifth Annual Conference of the Canadian Technical Asphalt Association (CTAA), November 2020.

Migliori, F., Ramond, G., Ballié, M., Brûlé, B, Exmelin, C., Lombardi, B., Samanos, J., Ferraro Maia, A., Such, C. and Watkins, S., “Correlations between the thermal stress cracking of bituminous mixes and the binders’ rheological characteristics,” Paper No. 046., Eurobitume Workshop 99 – Performance -Related Properties for Bituminous Binders, 1999.

Richards, F. J., “A Flexible Growth Function for Empirical Use. Journal of Experimental Botany,” Vol. 10, No 29, 1959, pp. 290-300.

Rowe, G.M., “*Interrelationships in Rheology for Asphalt Binder Specifications*,” 59th Annual Conference of Canadian Technical Asphalt Association, Winnipeg, Manitoba, November 16 to 19, 2014.

Rowe, G.M., Raposo, S.F. and Bredenhann, S., “*Defining the Rheological Type of Asphalt Binders for Use in Performance Related Specifications*,” Proceedings of the 13th Conference on Asphalt Pavements for Southern Africa, 15-18 October 2023.

Rowe, G.M. and Sharrock, M.J., “*The Direct Tension Test and The Behavior of Asphalt Binders at Low and Intermediate Temperatures*,” 3rd Eurasphalt & Eurobitume Congress, Vienna, 2004.

Appendix A

Draft Modified Procedure for Determining Asphalt Binder Yield Energy using a Dynamic Shear Rheometer (DSR)

Objective

This procedure uses a modified version of the Binder Yield Energy test procedure (BYET) to determine Binder Yield Energy (BYE) values for asphalt binders in the stiffness range of 1E+6 to 1E+8 Pa.

Procedure

- 1) Load an 8-mm DSR specimen on the 8-mm DSR parallel plates at elevated temperature (upper grade temperature should be acceptable) per the procedures provided in AASHTO T315 (ASTM D7175).
 - a. Stiffer binders can be “buttered” on the top and bottom of the specimen in order to promote better adhesion to plates.
- 2) Program the DSR to perform the following:
 - a. Allow a 10-minute “adhesion soak” time at the loading temperature. This will ensure that the binder bonds well to the plates.
 - b. Begin lowering the DSR temperature to test temperature at a rate of 5-7°C/minute. Simultaneously decrease the test gap from 2.00 mm to 1.75 mm at a constant rate.
 - c. Allow the sample to equilibrate at the test temperature for 5-10 minutes. Simultaneously decrease the test gap from 1.75 mm to the final test gap of 1.70 mm.
 - d. Set the top plate to continuously rotate at 0.05 RPM (~0.005 rad/s) for 20 minutes, recording a data point at each second.
 - i. Test time may vary based on binder type
 - e. Export the following data:
 - i. Point Number (i)
 - ii. Shear Strain (γ), %
 - iii. Shear Stress (τ), Pa
 - iv. Relaxation modulus ($G(t)$), Pa
- 3) Test 2 replicates per test temperature.

Analysis

- 1) Plot shear stress (y-axis) vs. shear strain (x-axis).
 - a. Fit a 4th order polynomial curve to the plot and record the equation.
 - b. For best fit, only plot curve to peak stress.
- 2) Plot the log of $G(t)$ and fit a power curve trendline. Record the constants a and b .
- 3) Determine the following data:
 - a. Peak Shear Stress (τ_{Peak})
 - b. Time to peak stress ($T_{\tau\text{Peak}}$) in seconds
 - c. Extension (E), mm:
 - i. $E = (0.000833333)(8\pi)(T_{\tau\text{Peak}})$
- 4) Calculate BYE by integrating the 4th order polynomial equation from the fitted curve to the peak:

$$\int_0^{Y_{\tau Peak}} ax^4 + bx^3 + cx^2 + dx + e$$

- 5) Report the G(t) at the peak load condition and the associated strain value.



aif
Asphalt Institute
Foundation[®]

Asphalt Institute Foundation
2696 Research Park Drive
Lexington, KY 40511
asphaltfoundation.org